



OPEN ACCESS

EDITED BY

Yu Qi,
Yanshan University, China

REVIEWED BY

Xianfeng Tan,
Chongqing University of Science and
Technology, China
Xixin Wang,
Yangtze University, China

*CORRESPONDENCE

Hao Wu,
✉ haowu@lzu.edu.cn

SPECIALTY SECTION

This article was submitted
to Economic Geology,
a section of the journal
Frontiers in Earth Science

RECEIVED 20 December 2022

ACCEPTED 12 January 2023

PUBLISHED 20 January 2023

CITATION

Wu H, Ban S, Du Z, Hao A, Li J, Wei G,
Zhang H, Zhang Y, Wu H and Li M (2023),
Controls on anomalously high porosity/
permeability of Middle Jurassic deeply
buried tight sandstones in the Taibei Sag,
Turpan-Hami Basin, northwestern China:
Implications for reservoir
quality prediction.
Front. Earth Sci. 11:1127807.
doi: 10.3389/feart.2023.1127807

COPYRIGHT

© 2023 Wu, Ban, Du, Hao, Li, Wei, Zhang,
Zhang, Wu and Li. This is an open-access
article distributed under the terms of the
[Creative Commons Attribution License
\(CC BY\)](https://creativecommons.org/licenses/by/4.0/). The use, distribution or
reproduction in other forums is permitted,
provided the original author(s) and the
copyright owner(s) are credited and that
the original publication in this journal is
cited, in accordance with accepted
academic practice. No use, distribution or
reproduction is permitted which does not
comply with these terms.

Controls on anomalously high porosity/permeability of Middle Jurassic deeply buried tight sandstones in the Taibei Sag, Turpan-Hami Basin, northwestern China: Implications for reservoir quality prediction

Hao Wu^{1,2*}, Shuyue Ban^{2,3}, Zhiwei Du^{1,2}, Aisheng Hao⁴, Jian Li⁴,
Guoliang Wei⁵, Hua Zhang⁵, Yunzhao Zhang⁶, Heng Wu⁷ and Mi Li⁸

¹Key Laboratory of Mineral Resources in Western China (Gansu Province), Lanzhou University, Lanzhou, China, ²School of Earth Sciences, Lanzhou University, Lanzhou, China, ³State Key Laboratory of Petroleum Resources and Prospecting, College of Geosciences, China University of Petroleum, Beijing, China, ⁴PetroChina Research Institute of Petroleum Exploration & Development, Beijing, China, ⁵Exploration and Development Research Institute, PetroChina Tuha Oilfield Company, Hami, China, ⁶School of Earth Sciences and Engineering, Xi'an Shiyou University, Xi'an, China, ⁷Hebei Key Laboratory of Strategic Critical Mineral Resources, HeBei GEO University, Shijiazhuang, China, ⁸School of Energy and Materials Engineering, Taiyuan University of Science and Technology, Taiyuan, China

The lower member of the Middle Jurassic Xishanyao Formation (J_2x^{1+2}) sandstones are significant exploratory targets for hydrocarbon resources in the Taibei Sag of the Turpan-Hami Basin, northwestern China. Formation of anomalously high porosity/permeability in deeply buried J_2x^{1+2} sandstones and reservoir quality prediction were investigated using a variety of petrographic analyses. These results show that the J_2x^{1+2} sandstones are mostly feldspathic litharenites and litharenites, which are characterized by moderate-to good sorting, silty to medium granularity, and point- to long grain contacts. The J_2x^{1+2} sandstone has low porosity (avg 6.0%) and permeability (avg 1.12 mD), but shows anomalously high porosity/permeability at depth interval of 3850–4050 m. There is a noticeable variation in pore types and sizes from intergranular-intragranular dissolution pores with a size mode of 2.0 μm in anomalously high porosity (AHP) sandstones, to major intragranular dissolution pores with a size mode of 0.5 μm in normally high porosity (NHP) sandstones, to most micropores with a size mode of 0.25 μm occurred in the normally low porosity (NLP) sandstones. The compaction is the main cause of porosity destruction, resulting in an average porosity loss of 89.6%. However, the authigenic minerals have relatively little influence on reservoir quality. The combination of nappe tectonics and well-sorted particles alleviated the compaction and thus preserved more intergranular pores in the AHP sandstones. Dissolution further increases the porosity and eventually forms the AHP sandstones. The strong carbonate-cemented facies (SCC), tightly compacted facies (TC), moderately compacted with moderate dissolution facies (MCMD), and weakly compacted with strong dissolution facies (WCSD) are determined in the J_2x^{1+2} sandstones. The sandstones with SCC and TC are recognized as the NLP reservoirs. The MCMD and WCSD correspond to the NHP and AHP reservoirs, respectively. The reservoir quality predicted using the constructed diagenetic facies charts is in good agreement with the photomicrograph observations and physical property tests. Additionally, the AHP

reservoirs are still developed in the deeply buried sandstones with depths larger than 4000 m.

KEYWORDS

anomalously high porosity, tight sandstones, diagenesis, diagenetic facies, reservoir quality prediction, Xishanyao Formation, Turpan-Hami Basin

1 Introduction

With the declines in production of conventional hydrocarbon resources and the quickly growing energy needs, the tight sandstone reservoirs have become one of the important exploration targets for petroleum industry (Law and Curtis, 2002; Desbois et al., 2011; Zou et al., 2012; 2013; Li et al., 2020). The tight sandstone reservoirs generally have poor physical property, which are characterized by highly variable reservoir quality in spatial distribution (Wu et al., 2022). Nevertheless, anomalously high porosity zone (AHPZ) is still developed in some tight sandstone reservoirs. The AHPZs are defined as the reservoirs having higher porosity relative to expected background values for their burial depth (Bloch et al., 2002; Nielsen et al., 2019), and can be widely developed across different geological periods, sedimentary facies and buried depth intervals in the various petroliferous basins (Sun et al., 2013; Cao et al., 2014; Yuan et al., 2015a; Wu et al., 2022). The determination of AHPZ is the central work of the genetic analysis and prediction of high-quality sandstone reservoirs, which are the sweet spots for hydrocarbon exploration, especially for deeply buried sandstone reservoirs.

The formation mechanism of anomalously high porosity (AHP) sandstones in the AHPZs has always been the concern for petroleum geologists. With the proposed dissolution mechanism by organic acid from kerogen maturation within the source rocks (Schmidt and McDonald, 1979; Surdam et al., 1989), many scholars believe that the secondary dissolution is the main reason for the formation of AHPZs (Weibel et al., 2019), while the primary pores have almost disappeared in the middle and deep layers (Zhong et al., 2003). Also, the effect of burial dissolution pores on AHPZ requires consideration of whether sandstone diagenesis occurs in an open or closed geochemical system (Gluyas and Coleman, 1992; Bjørlykke and Jahren, 2012; Yuan et al., 2015b; Luo et al., 2019). Secondary dissolution plays a significant effect on porosity-increase in open sandstone systems, whereas it has little effect on porosity-enhancing in closed sandstone systems (Yuan et al., 2015b). In addition, the formation of AHPZs in the mid-deep layers in some areas cannot be explained by secondary dissolution. The primary porosity-preserving mechanisms, such as hydrocarbon emplacement (Emery et al., 1993; Xia et al., 2020; Wu et al., 2022), high fluid pressure (Jin et al., 2011; Nguyen et al., 2013), microcrystalline quartz coatings (Aase et al., 1996; Worden et al., 2012), and clay coatings (Heald and Larese, 1974; Taylor et al., 2010; Zhou et al., 2016), have suggested to dominate the AHPZ formation. The deeply buried sandstone reservoirs of the lower member of the Middle Jurassic Xishanyao Formation (J_2x^{1+2}) in the Taibei Sag of Turpan-Hami Basin show anomalous high porosities than expected background values for the burial depth, and more primary intergranular pores dominate these high-porosity sandstones, indicating that high porosity may be related to the primary porosity-preserving capacity. However, the mechanisms previously mentioned cannot explain the development of primary intergranular pores in the deeply buried J_2x^{1+2} sandstones,

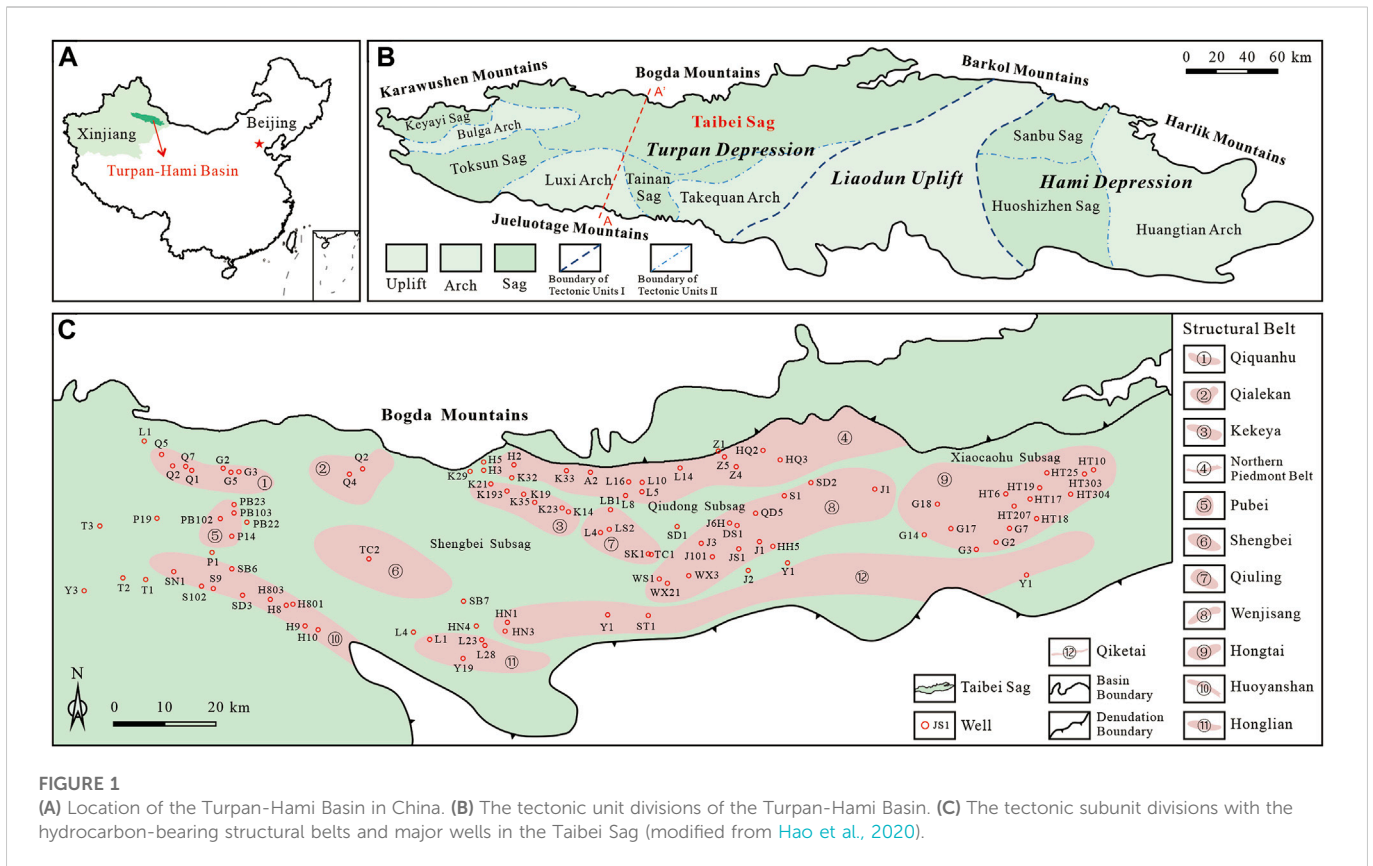
the cause responsible for the formation of AHPZ needs to be rethought and clarified.

The reservoir quality is the comprehensive results of depositional environment and diagenetic modifications, which is difficult to predict due to the strong heterogeneity. The diagenetic facies that indicates the final state of reservoir is generally used to predict and evaluate the reservoir quality (Ozkan et al., 2011; Lai et al., 2018). At present, many studies have been done on correlating the diagenetic facies with well logs to evaluate reservoir quality (Cui et al., 2017; Lai et al., 2018; Wu et al., 2020; Li et al., 2022). The same AHPZ generally has different genetic types of sandstone reservoirs, including AHP sandstone, normally high porosity (NHP) sandstone, and normally low porosity (NLP) sandstone (Hao et al., 2020). However, there are few studies to correlate the diagenetic facies with different types of sandstone reservoirs and then use the corresponding logging response readings to predict the reservoir quality.

The sandstone of the Middle Jurassic Xishanyao Formation is important tight hydrocarbon reservoir in the Taibei Sag of Turpan-Hami Basin. A new chapter of Jurassic hydrocarbon exploration was opened with the acquisition of industrial oil flow in the Sanjianfang Formation by the scientific exploration well TC one in the Turpan-Hami Basin (Zhai et al., 2016). The hydrocarbon exploration currently focuses on the sandstones of the upper member of Xishanyao Formation, Sanjianfang Formation and Qiketai Formation in the forward structural belt around the sub-sags (Ni et al., 2019; Li et al., 2021). The lithologic hydrocarbon reservoir within coal-bearing source rocks of the J_2x^{1+2} and the lower Jurassic as an important replacement field, however, there is a lack of systematic studies on the quality evaluation and prediction of these sandstone reservoirs (Hao et al., 2022; He et al., 2022; Liang et al., 2022). Therefore, taking the J_2x^{1+2} tight sandstones as a typical example, this paper studied the mechanism responsible for the formation of AHPZ and predicted distribution of high-quality reservoirs. The study mainly focused on the following objectives: 1) to characterize reservoir lithologies, reservoir properties and diagenetic mineralogy, and contradistinguish AHP from NHP and NLP sandstones; 2) to identify the key controlling factors for the formation of AHPZ; 3) to associate different types of diagenetic facies with (AHP, NHP, and NLP) sandstone reservoirs; and 4) to construct the logging responses of (AHP, NHP, and NLP) sandstones and predict reservoir quality. The results of this work will be expected to have a great significance for reservoir quality evaluation and prediction, and provide reference for exploring and developing hydrocarbon reservoirs in analogous geological settings.

2 Geological settings

The Turpan-Hami Basin, located in northwest China (Figure 1A), is an E-W elongated intermontane basin nestled in the North Tian Shan orogenic belt and covers an area of 5.35×10^4 km² (Chen et al.,

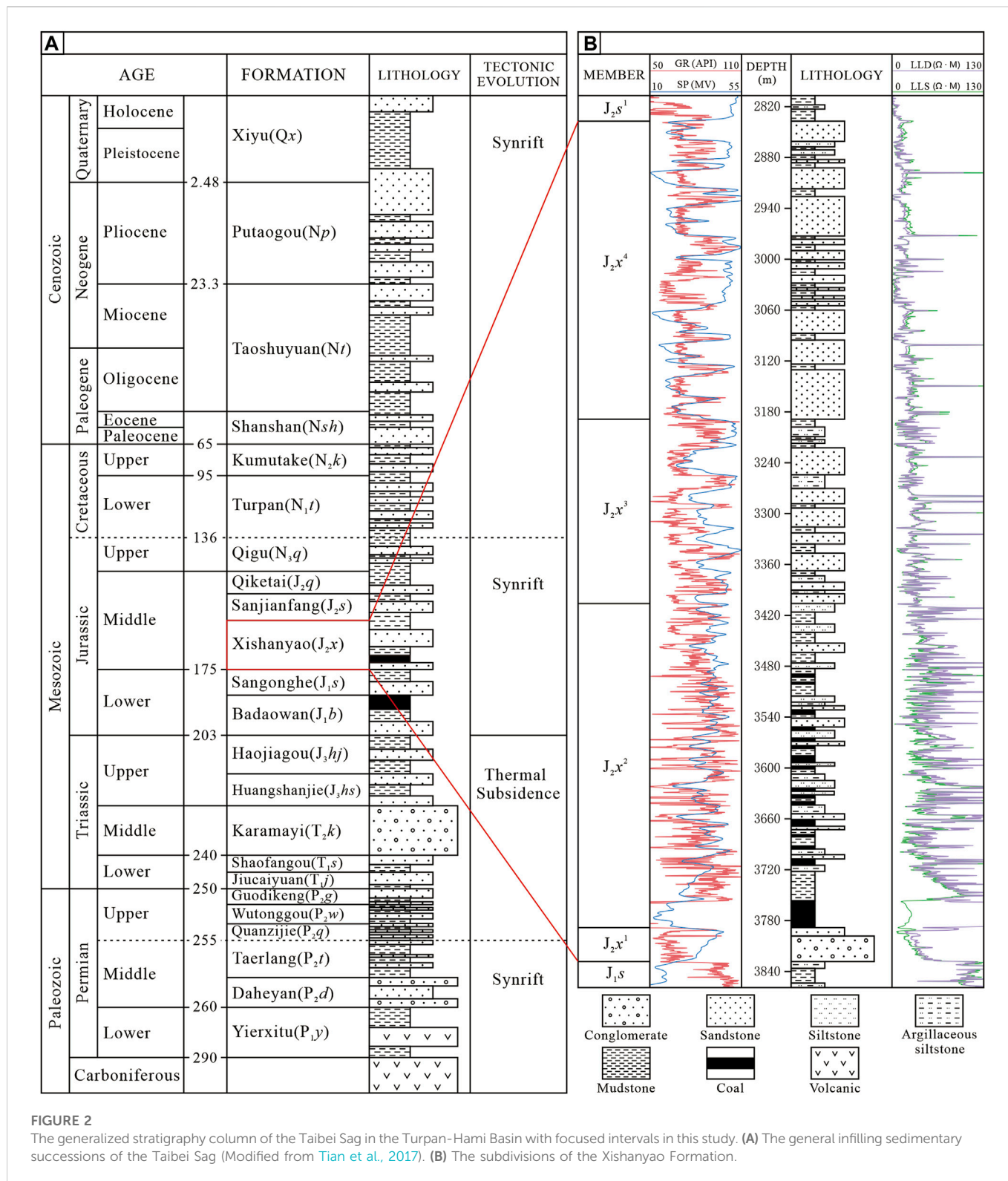


2001; Greene et al., 2004; Han et al., 2016; Shen et al., 2020). It developed on the folded basement of the Early Paleozoic oceanic crustal fragments and accretionary metasedimentary rocks, and mainly contains non-marine Mesozoic-Cenozoic fills (Carroll et al., 1990; Allen et al., 1995; Greene et al., 2005; Xia et al., 2012). The present boundaries of Turpan-Hami Basin are defined by Jueltuotage mountains to the south, Barkoland and Bogda mountains to the north, Harlik mountains to the east, and Karawushen mountains to the west (Figure 1B). The Turpan-Hami Basin consists of three first-order tectonic units from west to east, i.e., Turpan depression, Liaodun uplift, and Hami depression (Figure 1B). The Taibei Sag as the study area is the secondary structural unit in the Turpan depression and covers approximately 1×10^4 km² (Figure 1C). According to the tectonic evolution characteristics, the Taibei Sag can be further divided into twelve positive structural subunits such as the northern piedmont structural belt and Hongtai structural belt, and three negative structural subunits such as Shengbei subsag, Quidong subsag and Xiaocaohu subsag (Figure 1C).

The evolution of the Turpan-Hami Basin during the Carboniferous-Quaternary is generally divided into four phases (Figure 2A) (Tian et al., 2017): 1) The first syn-rift phase was from Carboniferous to Middle Permian, during which sediments were dominated by fluvial-lacustrine depositional system; 2) The thermal subsidence phase was from Late Permian to Triassic, during which sediments were dominated by fluvial depositional system; 3) The second syn-rift phase lasted throughout the Jurassic, during which sediments were dominated by fluvial-swamp-lacustrine depositional system; and 4) The third syn-rift phase spanned the Cretaceous to Quaternary, during which sediments were dominated

by fluvial-swamp depositional system. In addition, the Jurassic structural layers were mainly depicted by decollement along coal-bearing strata (Gao et al., 2018).

At present, the discovered hydrocarbon resources are mainly concentrated in the Taibei Sag. From base to top, the sedimentary successions in the Taibei Sag are represented by the Carboniferous, Permian, Triassic, Jurassic, Cretaceous, Paleogene, Neogene, and Quaternary strata (Figure 2A), and a maximum thickness can reach up to approximately 9000 m (Wu and Zhao, 1997; Zhang et al., 2018; Ni et al., 2019). The main petroliferous intervals originate from the Jurassic deposited during the second syn-rift stage (Tian et al., 2017), which can be divided into Lower Jurassic Badaowan Formation (J_{1b}) and Sangonghe Formation (J_{1s}), Middle Jurassic Xishanyao Formation (J_{2x}), Sanjianfang Formation (J_{2s}) and Qiketai Formation (J_{2q}), and Upper Jurassic Qigu Formation (J_{3q}) and Kalaza Formation (J_{3k}), from bottom to top (Figure 2A). The J_{2x} comprises high quality reservoir rocks and source rocks (Chen et al., 2001; Ni et al., 2019), and is divided into four members as J_{2x}¹, J_{2x}², J_{2x}³, and J_{2x}⁴ from bottom to top (Figure 2B). Overall, the J_{2x} is mainly composed of siltstones, sandstones, mudstones, and thick coal seams deposited in delta-lacustrine system (Shao et al., 2003), or rather, fan delta deposits are developed in the northern Taibei Sag, and braided-river delta deposits are developed in the southern part. The J_{2x}¹ mainly consists of sandstone and fine conglomerate. The J_{2x}² is composed of siltstone, mudstone, carbonaceous mudstone, and coal seam. The J_{2x}³ is characterized by the interbeds of mudstone, light gray sandstone, and siltstone in different thickness. The J_{2x}⁴ contains gray massive sandstone, glutenite, and gray-green mudstone (Figure 2B). The average vitrinite reflectance R_o of coal-bearing source rocks varies from 0.6% to



0.9%, signifying source rocks are at a low mature to mature stage (Chen et al., 2001; Tian et al., 2017). The J_2x sediments mainly sourced from the Jueluotage mountains in south and Bogda mountains in north (Greene et al., 2005; Ji et al., 2017; Hao et al., 2021). This paper focuses on the deeply buried tight sandstones in the lower part of the Middle Jurassic Xishanyao Formation (J_2x^{1+2}) in the Taibei Sag.

3 Samples and methods

A total of 4490 core samples from 253 wells were studied in petrography and mineralogy, in order to elucidate the controlling factors for the formation of AHPZ of the J_2x^{1+2} tight sandstones in the Taibei Sag.

TABLE 1 The detrital components, major diagenetic minerals and grain sizes of different types of sandstone reservoirs in the Taibei sag.

Well name	Depth (m)	Porosity (%)	Permeability (mD)	Lithology	Reservoir type	Detrital component (%)			Carbonate cement	XRD-derived relative clay minerals (%)					Grading analysis		
						Quartz	Feldspar	Rock fragments		I/S	Illite	Kaolinite	Chlorite	S	MGS (mm)	AGS (mm)	SC
G12	4009.95	13.3	0.224	fine sandstone	AHP	29.2	29.2	41.6	2.6	14	21	52	13	13	0.17	0.12	1.98
H803	3996.71	12.8	5.485	sandy conglomerate	AHP	30.0	14.5	54.4	0.2	5	18	56	21	20	0.30	0.23	1.80
H803	3997.18	12.4	4.238	sandy conglomerate	AHP	32.6	14.1	52.3	0.2	6	13	47	34	20	0.23	0.18	1.91
H803	3998.63	12.6	5.688	sandy conglomerate	AHP	28.6	16.5	53.9	0.2	5	15	42	38	10	0.29	0.22	2.02
H803	4000.12	13.3	3.940	sandy conglomerate	AHP	32.3	12.9	53.8	0.2	3	12	56	29	20	0.23	0.17	1.99
P103	3904.44	11.6	0.670	coarse sandstone	AHP	21.6	29.6	48.8	1.0	14	10	45	31	20	0.11	0.06	2.73
P103	3936.46	11.1	1.030	medium sandstone	AHP	22.5	26.9	49.4	1.2	9	18	46	27	10	0.19	0.11	1.84
Y1	4055.68	9.8	0.980	fine sandstone	AHP	26.0	25.0	48.0	1.5	5	11	54	30	30	0.20	0.16	1.74
Y1	4058.78	10.7	0.991	fine sandstone	AHP	27.0	26.0	48.0	0.8	2	13	40	45	20	0.19	0.16	1.80
Y1	4059.55	11.2	1.330	fine sandstone	AHP	27.0	27.0	46.0	1.2	1	14	42	43	30	0.25	0.19	1.70
Y1	4062.47	10.4	1.170	fine sandstone	AHP	29.0	26.0	46.0	0.8	2	11	40	47	20	0.23	0.17	1.72
G12	4007.93	9.5	1.244	fine sandstone	NHP	28.7	27.7	42.6	0.1	12	15	64	9	18	0.15	0.10	2.22
G12	4008.70	7.3	3.790	fine sandstone	NHP	30.1	29.1	41.0	2.5	14	13	67	6	16	0.27	0.18	2.12
G12	4009.41	9.5	0.489	fine sandstone	NHP	28.4	27.3	44.3	1.0	13	19	55	13	16	0.16	0.09	2.57
G12	4010.61	7.8	0.297	fine sandstone	NHP	26.6	27.6	45.7	2.1	14	19	53	14	17	0.18	0.12	2.27
H801	3867.69	7.7	0.060	fine sandstone	NHP	25.0	22.8	47.9	1.1	22	23	34	21	66	0.08	0.06	2.35
H801	3868.25	7.1	0.359	fine sandstone	NHP	21.4	19.0	58.4	2.0	10	21	48	21	20	0.28	0.19	2.00

(Continued on following page)

TABLE 1 (Continued) The detrital components, major diagenetic minerals and grain sizes of different types of sandstone reservoirs in the Taibei sag.

Well name	Depth (m)	Porosity (%)	Permeability (mD)	Lithology	Reservoir type	Detrital component (%)			Carbonate cement	XRD-derived relative clay minerals (%)					Grading analysis		
						Quartz	Feldspar	Rock fragments		I/S	Illite	Kaolinite	Chlorite	S	MGS (mm)	AGS (mm)	SC
H801	3869.65	9.2	0.526	sandy conglomerate	NHP	20.9	17.6	60.5	0.8	23	13	44	20	20	0.41	0.31	2.60
L1	3935.86	7.6	0.440	medium sandstone	NHP	30.0	24.0	46.0	1.3	6	37	36	21	20	0.33	0.30	1.59
P103	3902.37	8.9	4.840	coarse sandstone	NHP	23.3	26.7	48.9	1.0	14	16	41	30	20	0.21	0.12	1.76
Y1	4057.86	9.2	0.362	fine sandstone	NHP	26.0	25.0	48.0	1.1	4	11	44	41	20	0.18	0.14	1.83
J3	4046.57	5.6	2.515	medium sandstone	NLP	30.9	19.2	50.1	1.3	15	72	11	2	30	0.37	0.24	2.25
J3	4048.78	4.8	0.138	fine sandstone	NLP	29.5	21.1	49.6	0.4	23	45	27	5	30	0.24	0.18	1.96
K31	3857.52	5.4	0.087	fine sandstone	NLP	27.4	21.1	50.5	0.6	64	36	0	0	19	0.26	0.16	2.30
K31	3859.68	5.8	0.089	fine sandstone	NLP	25.3	24.2	50.6	0.2	50	50	0	0	16	0.24	0.16	2.33
K31	3862.98	5.8	0.042	medium sandstone	NLP	26.3	25.2	48.4	0.1	33	67	0	0	18	0.27	0.17	2.38
K31	4011.87	3.8	0.003	coarse sandstone	NLP	23.2	17.9	59.0	0.1	69	31	0	0	12	0.22	0.16	2.97
K31	4012.62	4.5	0.012	coarse sandstone	NLP	26.3	23.2	50.5	0.6	62	37	0	1	12	0.29	0.18	2.63
K31	4014.97	3.0	0.012	coarse sandstone	NLP	26.3	25.2	48.4	0.4	55	44	0	1	13	0.20	0.13	2.45
K31	4016.19	4.6	0.104	coarse sandstone	NLP	24.2	16.9	59.0	0.5	61	38	0	1	12	0.28	0.17	2.77
K32	3856.06	5.0	0.193	coarse sandstone	NLP	23.7	10.3	66.0	1.2	8	91	0	1	10	0.40	0.28	2.60
L4	3959.97	1.5		fine sandstone	NLP	26.0	23.0	52.0	0.5	10	22	49	19	10	0.05	0.03	3.49

I/S, Illite/smectite mixed layer; S, The proportion of smectite in I/S; MGS, Median grain size; AGS, Average grain size; SC, Sorting coefficient.

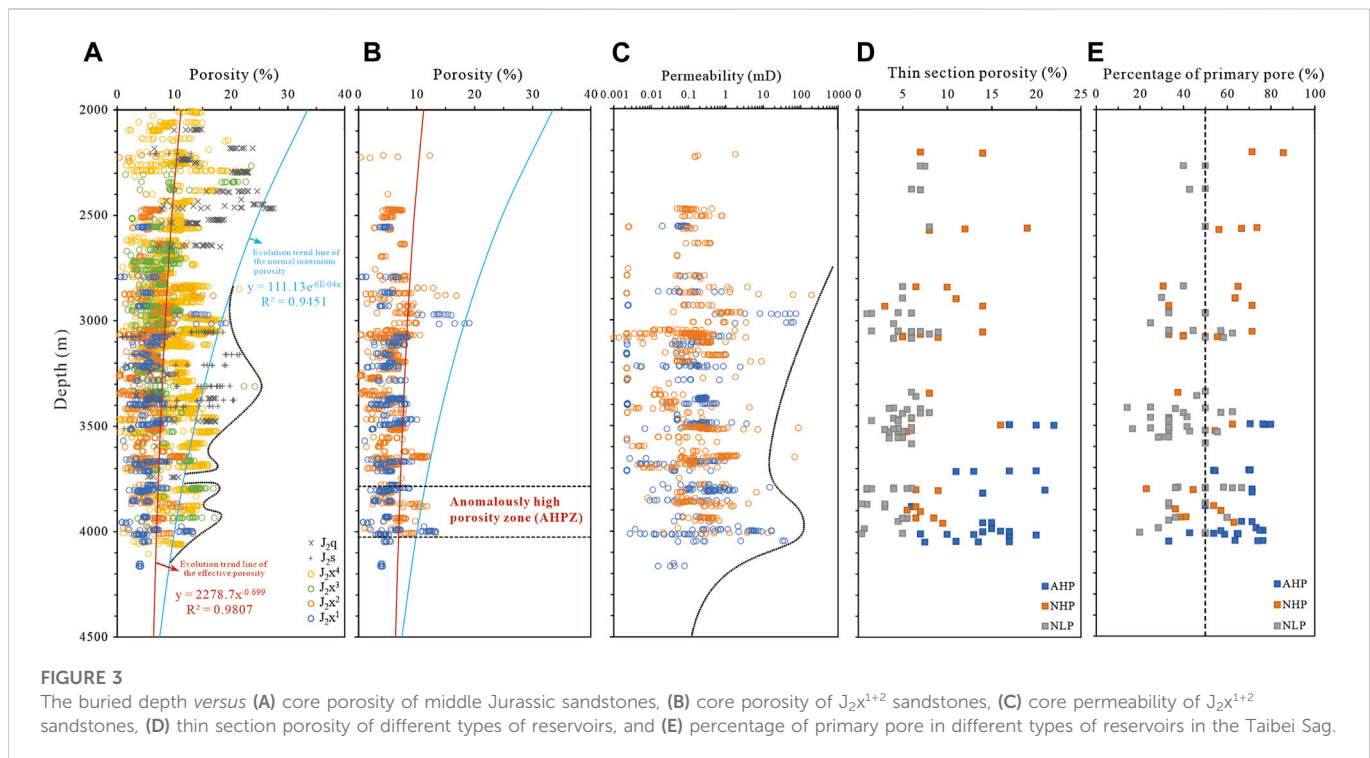


FIGURE 3

The buried depth versus (A) core porosity of middle Jurassic sandstones, (B) core porosity of J_2x^{1+2} sandstones, (C) core permeability of J_2x^{1+2} sandstones, (D) thin section porosity of different types of reservoirs, and (E) percentage of primary pore in different types of reservoirs in the Taipei Sag.

The red epoxy resin-impregnated thin sections were prepared for determining the detrital mineralogy, diagenetic mineralogy, pore types and the corresponding thin-section porosity of samples by counting 300 points per thin slices with Olympus BX51 digital transmission microscope (Stroker et al., 2013). Thin sections were partly stained with Alizarin Red S and K-ferricyanide for identifying the carbonate minerals (Dickson, 1965).

Sixty-two samples were gold-coated and performed on the Quanta 200F scanning electron microscopy (SEM) with a resolution of 1.2 nm to observe diagenetic minerals (especially authigenic clay minerals), pore types and morphology at micro to nano-scales.

The clay fraction mineralogy of 120 samples were analyzed using X-ray diffraction (XRD), which was performed on a D8 DISCOVER X-ray diffractometer at 40 mA and 40 kV. The specific procedures for sample preparation and XRD measurement were according to Hillier (2003) and Clarkson et al. (2013).

Two hundred and thirty-eight samples were selected for granulometry measurement to determine the grain size and sorting degree of grains, which were conducted on an MS 2000 laser granularity analyzer. The specific procedures for preparation, analysis and interpretation of these samples were according to Amireh (2015) and Zhang et al. (2019).

The mercury injection capillary pressure (MICP) analysis was performed to characterize the pore structure characteristics such as pore size distribution (PSD) and pore-throats connectivity. 120 samples were conducted by using an AutoPore IV9500 mercury porosimeter. The maximum pressure of mercury injection is 35 MPa, corresponding to a pore-throat radius of 20 nm (Washburn, 1921).

The porosities and permeabilities of 10902 core plug samples were measured by helium injection, which were performed on a Ultrapore-200A porosimeter and an Ultra-PermTM200 permeameter. Before the experiments, these core plugs were cleaned with a mixed solution of

alcohol and trichloromethane to remove the residual oil and then dried with a vacuum at 110°C for 24 h.

4 Results

4.1 Detrital mineralogy

The detrital compositions of the studied sandstones comprise 6.4%–55.9% quartz (Q), 4.1%–35.4% feldspar (F) and 19.2%–85.1% rock fragment (R), showing that the sandstones are primarily feldspathic litharenites and litharenites according to the classification scheme presented by Folk (1980), with an average component of $Q_{29.3}F_{21.3}R_{49.4}$ (Table 1). There is no significant difference between the J_2x^1 and J_2x^2 sandstones in detrital component. Both J_2x^1 and J_2x^2 sandstones are enriched in lithic, with lithic populations comprising sedimentary fragments (avg 1.5%), metamorphic fragments (avg 4.5%), igneous fragments (avg 27.5%), and volcanoclastic fragments (avg 14.8%).

The J_2x^{1+2} reservoirs are mostly silt- to medium-grained sandstones with moderate- to good sorting. The framework grains are primarily subrounded-subangular and subangular, and mostly range from point to linear contacts.

4.2 Reservoir properties

4.2.1 Porosity and permeability

The porosity of studied sandstone samples has an average value of 6.0% with a range from 0.4% to 19.1%, and the permeability has an average value of 1.12 mD with a range from 0.001 to 197 mD. In general, the J_2x^{1+2} belongs to the tight sandstone reservoirs, since a total of 89.2% of samples have a porosity of less than 10% and

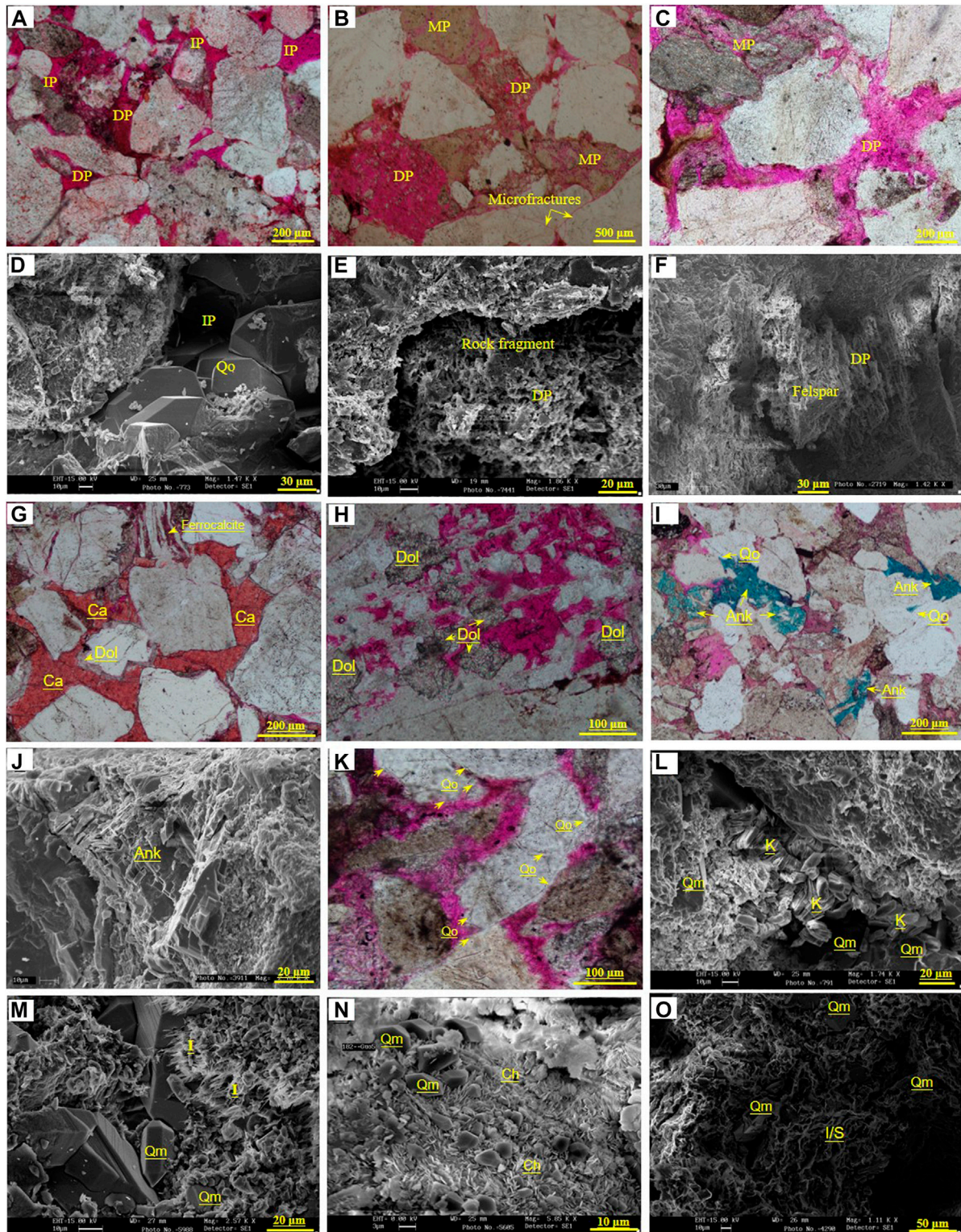


FIGURE 4

Photomicrographs showing typical pore types and diagenetic minerals of the J_2x^{1+2} sandstone reservoirs in the Taibei sag. (A) PPL view showing mixed pores of primary intergranular pores and dissolution pores (Well H803, 3998.59 m). (B) PPL showing intragranular dissolution pores and a small number of micropores (Well K23, 3991.77 m). (C) PPL showing micropores formed by interstitial materials dissolution (Well K23, 3992.69 m). (D) SEM image showing the remaining intergranular pore after quartz overgrowths fillings (Well H803, 3998.63 m). (E) SEM image showing the dissolution pores of rock fragment (Well H801, 3865.65 m). (F) SEM image showing the feldspar dissolution pores (Well YB3, 3836.39 m). (G) PPL view showing the early poikilitic calcites (Well H801, 3868.25 m). (H) PPL image viewing the intragranular dissolution pores were replaced by the dolomites (Well K33, 3801.94 m). (I) PPL image showing the dissolved frameworks replaced by ankerites partly or entirely (Well L2, 3473.01 m). (J) SEM image showing the ankerite cement with rhombohedral crystals (Well G12, 4009.36 m). (K) PPL image showing the quartz overgrowths (Well K31, 4012.55 m). (L) SEM image showing the intergranular pores filled by the kaolinite aggregates (Well H803, 4041.04 m). (M) SEM image showing pore-filling euhedral quartz crystals and illites (Well J3, 4125.75 m). (N) SEM image showing the euhedral quartz crystals and chlorites (Well G5, 3650.02 m). (O) SEM image showing the I/S mixed layers (Well K23, 3991.14 m). IP- intergranular pores; DP- dissolution pore; MP- micropore; Qo- quartz overgrowths; PPL- plane-polarized light; SEM- scanning electron microscope; Ca- calcite; Dol- dolomite; Ank- Ankerite; K- kaolinite; I- illite; I/S- illite/smectite mixed layer; Ch- Chlorite.

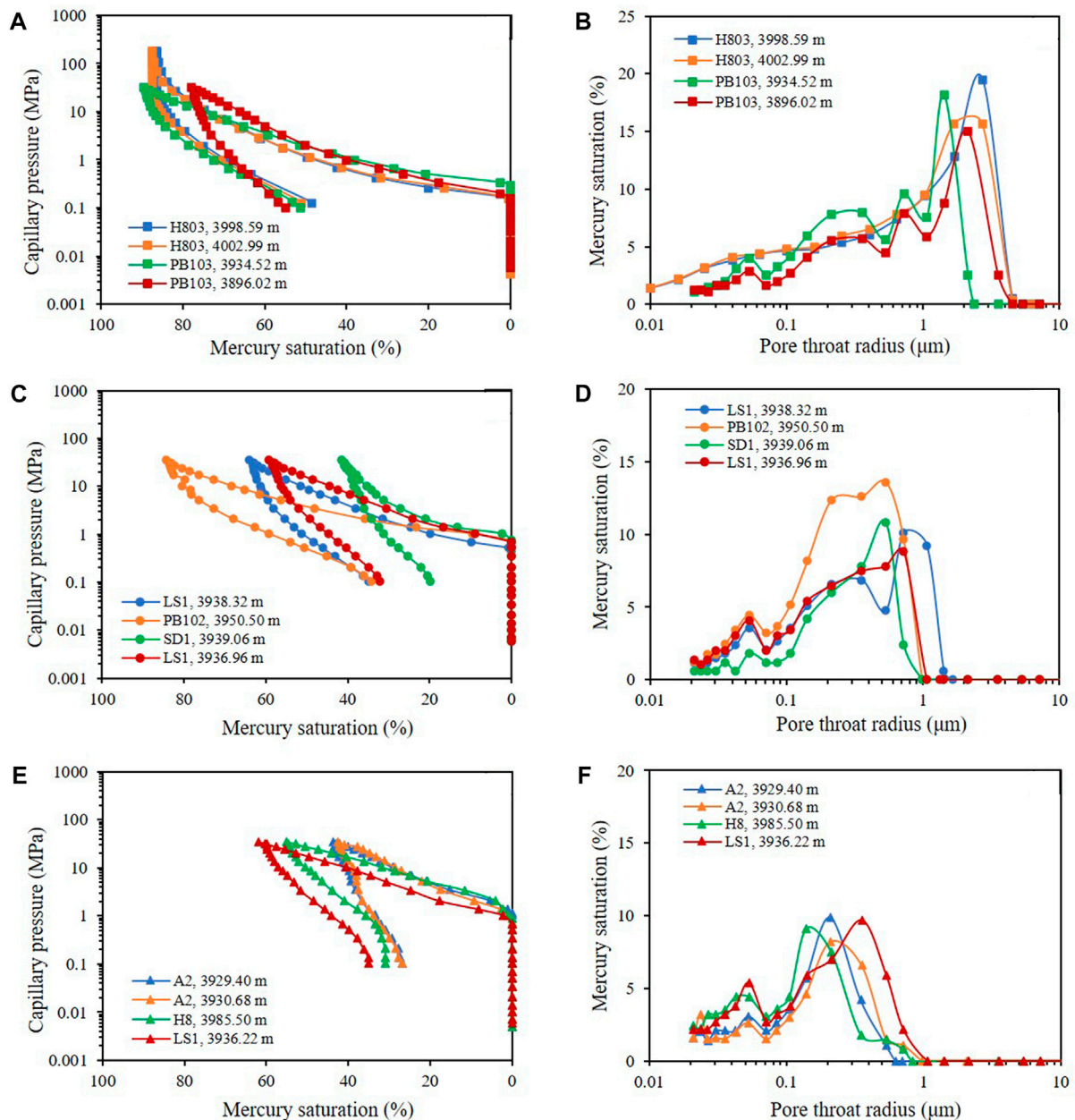


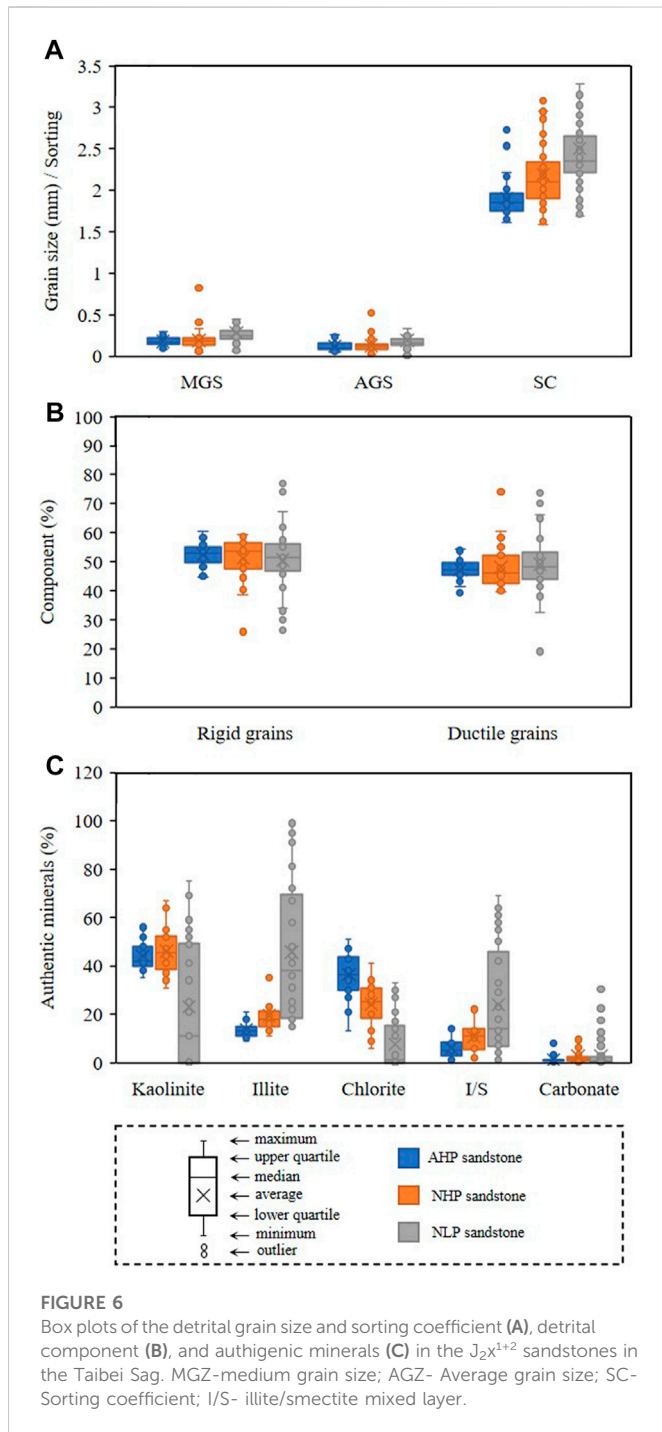
FIGURE 5
MICP curves (A, C, E) and corresponding pore-throat size distributions (B, D, F) of different types of sandstones in the Taibei Sag. (A, B)-AHP sandstones. (C, D)-NHP sandstones. (E, F)-NLP sandstones.

permeability of less than 1 mD. The results also showed that J_{2x^1} and J_{2x^2} have similar physical property distributions, with an average porosity and permeability of 5.8% and 1.31 mD, and 6.3% and 0.97 mD, respectively.

4.2.2 AHPZ determination

Determination of effective porosity and normal maximum porosity is the core work for identifying AHPZ and predicting reservoir quality. The effective porosity can separate the effective reservoir from the ineffective reservoir, and can be determined using the specific method proposed by Wang et al. (2009). The log-interpreted porosities of different oil-bearing layers and dry

layers were used to determine the lower limit of effective porosity at depth interval of 300 m in the range of 2000–4500 m by using the cumulative distribution function (Wang et al., 2009; Wu et al., 2022). There existed very significant power correlation between the lower boundary of effective porosity and depth with a coefficient of determination of 0.98. The lower boundary of effective porosity is displayed as the solid red line in Figure 3A. The normal maximum porosity was determined using the specific method proposed by Bloch et al. (2002). In addition to the 1203 core porosity data for J_{2x^1} and J_{2x^2} , a total of 9699 core porosity data from Middle Jurassic J_{2x^3} , J_{2x^4} , J_{2s} and J_{2q} were used to determine the normal maximum porosity by plotting the histogram of the porosity distribution per 300 m depth



interval (Bloch et al., 2002). There lies in an exponential relationship between the normal maximum porosity and depth with a coefficient of determination of 0.95. The evolution trend line of normal maximum porosity is shown as the solid blue line in Figure 3A.

The normal maximum porosity evolution trend line combined with the porosity envelope indicates that the depth intervals of 3000–3700 m and 3800–4050 m exhibit AHP (Figure 3A). The J_2x^1 and J_2x^2 show anomalously high measurements at depth interval of 3850–4050 m (Figures 3B, C). The porosity lower than the boundary of effective porosity and greater than the boundary of normal maximum porosity is defined as NLP and AHP sandstones, respectively. The sandstones between the lower boundary of

effective porosity and the maximum porosity boundary is called NHP sandstones.

4.2.3 Pore types and thin-section porosity

The primary intergranular pores, secondary dissolution pores and micropores are recognized in the J_2x^{1+2} sandstones based on SEM and thin section observations (Figure 4). The primary intergranular pores are characterized by smooth pore edge, regular shape, and flat grain edge (Figures 4A, D). Secondary dissolution pores with irregular shapes are mostly intragranular dissolution of feldspars and rock fragments (Figures 4A, B, E, F), and a small amount dissolution pores of grain margins and interstitial materials (Figure 4C). Micropores were generally occurred in matrix and clay-dominated intercrystalline pores (Figures 4C, L–O) and weak intragranular dissolution pores (Figure 4C). The reservoir space assemblages of different types of sandstones in the AHPZ are different. The results show that there is a noticeable variation in pore types from intergranular-intragranular dissolution pores in the AHP sandstones, to major intragranular dissolution pores in the NHP sandstones, to most micropores happened in the NLP sandstones. In the AHP sandstones, thin section porosity of primary pores ranges from 1.0% to 17.0%, with an average of 9.33% (Figure 3D). The proportion of primary pores in the AHP sandstones can reach 63.5% on average (Figure 3E), indicating that primary pores dominate the development of the AHPZ in the J_2x^{1+2} sandstones.

4.3 Diagenetic mineralogy

The J_2x^{1+2} sandstones in the AHPZ have various diagenetic minerals, including carbonates, clay minerals, and quartz cements. The volume of carbonate cements ranges from 0.1% to 24.4%, with an average of 2.1%. The carbonate cements are composed of calcite (Figure 4G), dolomite (Figure 4H), and ankerite (Figures 4I, J). The calcite generally filled the intergranular pores and occurred as a sparry or poikilitic crystals, which represent the early stage of precipitation. The dolomite and ankerite represent the late stage of precipitation, and commonly occurs in the form of filling intragranular or intergranular pores and replacing framework grains (Figures 4H, I). Authigenic quartz is not as widespread as clay and carbonate cements in the J_2x^{1+2} sandstones, with an average of less than 0.5%. Quartz cements occurred in syntaxial overgrowths (Figure 4K) and euhedral quartz crystals, which generally filled the intergranular or intragranular pores, and often appears together with the illite/smectite (I/S) mixed layers, illite, chlorite and kaolinite (Figures 4M–O).

The volume of authigenic clay cement ranges from 0.5% to 3.0%, with an average of 1.2%. The clay cement includes kaolinites (Figure 4L), illites (Figure 4M), chlorites (Figure 4N), and I/S mixed layers (Figure 4O), and their contents vary significantly in the AHP, NHP and NLP sandstones (Table 1). The kaolinite and chlorite dominate the clay cements in the AHP sandstones, which averaged 44.2% and 36.5% of the total clay mineral content, respectively. The kaolinite, chlorite and illite dominate the clay cements in the NHP sandstones, which averaged 46.2%, 24.1% and 19.4% of the total clay mineral content, respectively. However, the illite and I/S mixed layer are the major clay cements in the NLP sandstones, which averaged 59.0% and 30.6% of the total clay mineral content, respectively.

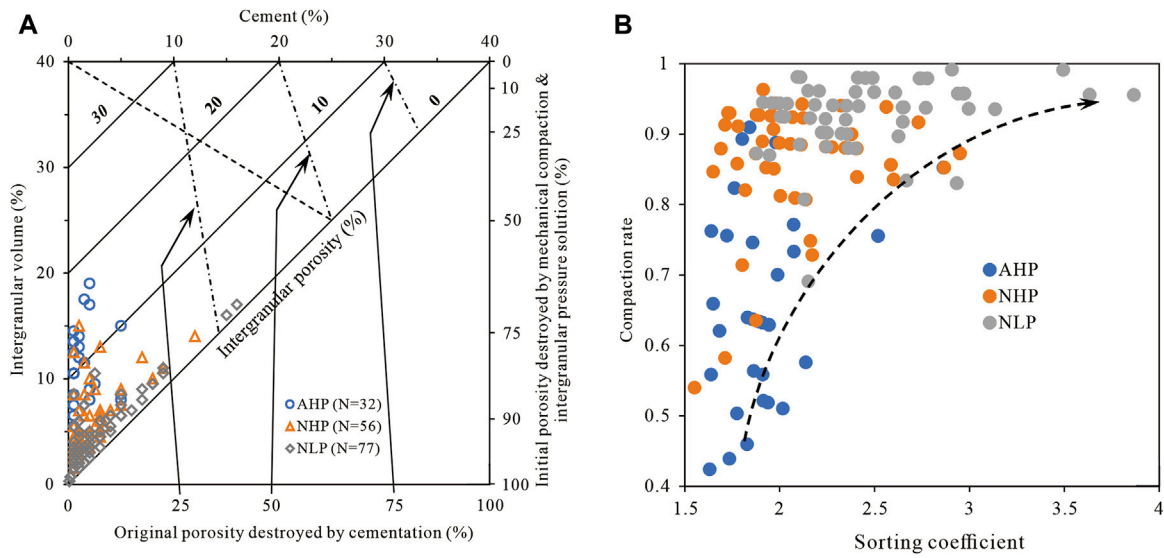


FIGURE 7 (A) Plot of the effect of compaction and cementation on porosity loss in the J_2x^{1+2} sandstones (modified from Houseknecht, 1987; Ehrenberg, 1989). (B) Cross-plot showing the relationship between the sorting coefficient and the compaction rate.

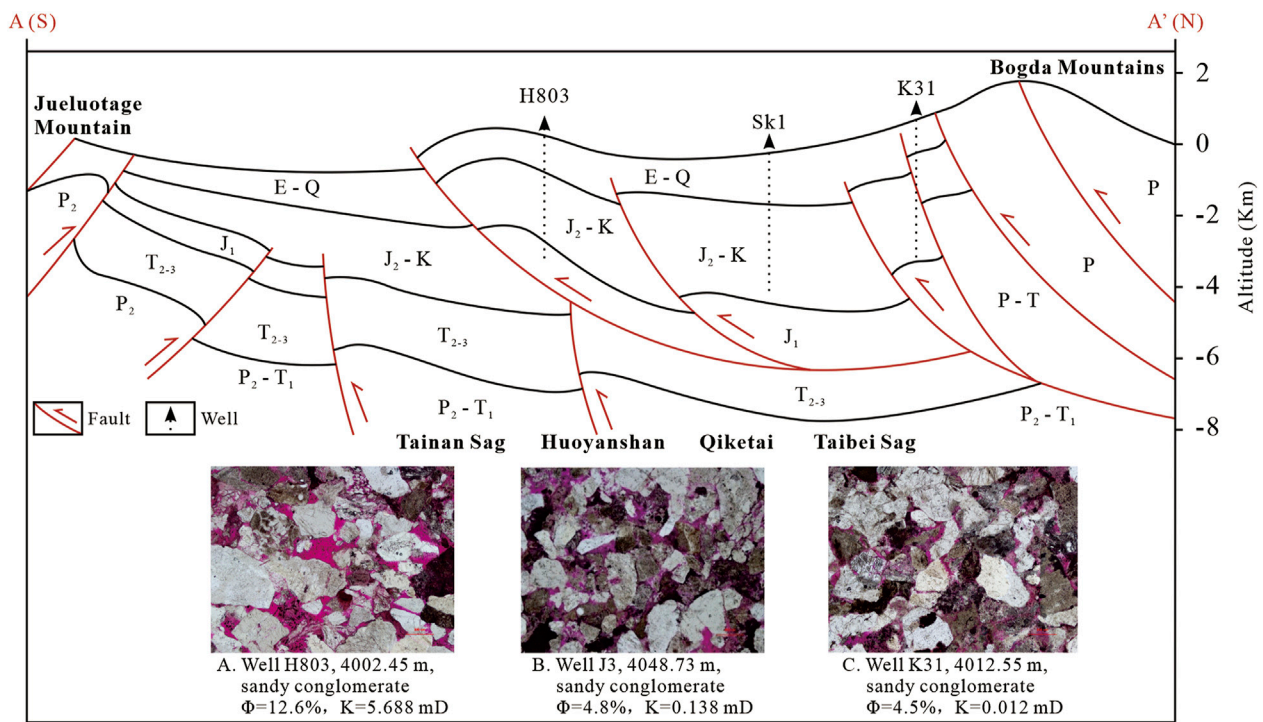


FIGURE 8 Simplified profile sketch showing the nappe tectonics and its influence on compaction (modified from Wu and Zhao, 1997; Shou et al., 2005). The profile location is shown in Figure 1.

4.4 MICP curves and PSD

The MICP curves of AHP, NHP and NLP samples are shown in Figure 5. The MICP curves of AHP and NHP samples increases

gradually from the beginning to the end with a “plateau-trend” stage at the early period of mercury injection compared with NLP samples (Figures 5A, C), indicating that the pore-throat sorting of AHP and NHP sandstones is better than that of NLP sandstones. The maximum

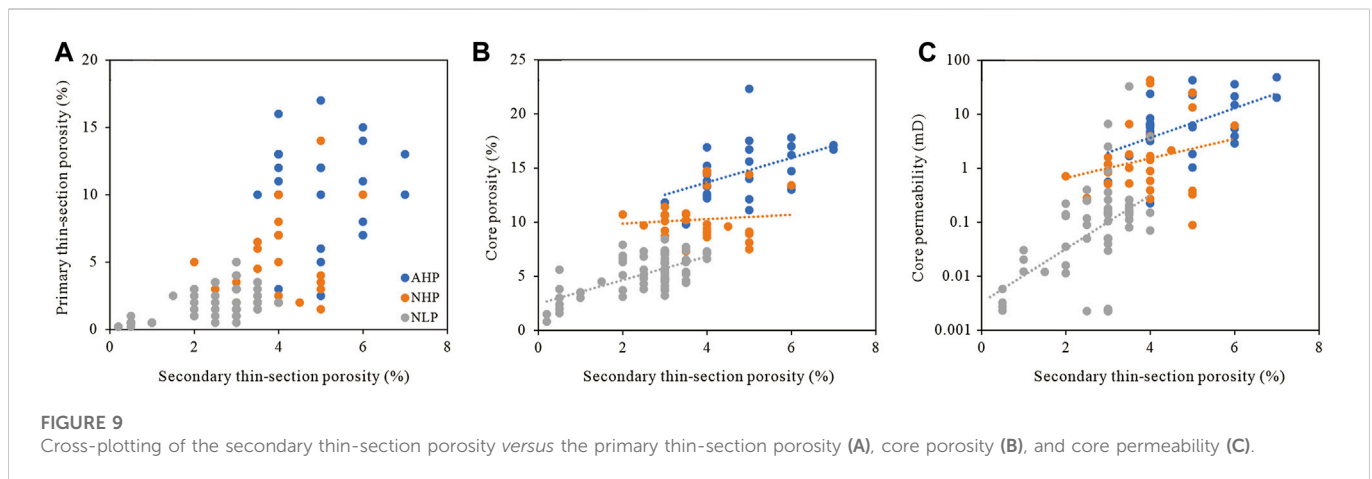


FIGURE 9 Cross-plotting of the secondary thin-section porosity versus the primary thin-section porosity (A), core porosity (B), and core permeability (C).

pore-throat radius (R_m) and medium pore-throat radius (R_{50}) decrease with increasing the threshold pressures (P_d) and medium saturation pressure (P_{50}) from AHP to NHP to NLP samples, signifying that the larger pore throats exist in the AHP sandstones. The P_d is less than 0.3 MPa in the AHP samples and greater than 0.5 MPa in the NHP and NLP samples. Furthermore, the maximum mercury saturation of AHP samples (avg 87.3%) was higher than that of NHP and NLP samples.

The PSD is wide, ranging from 21 nm to 10 μm (Figures 5B, D, F), and shows significant differences among AHP, NHP and NLP sandstones. The PSD of AHP samples shows a significant unimodal pattern and mainly ranges from 0.1 μm to 10 μm with a mode of 2 μm (Figure 5B). The PSD of NHP and NLP samples has similar distribution characteristics and shows a bimodal pattern. The smaller pore-throats size (minor peak) of NHP and NLP samples are ranging from 21 nm to 0.08 μm with a mode of 0.05 μm . Although the larger pore-throats size (primary peak) of both NHP and NLP are distributed between 0.1 μm and 1 μm , the mode of NHP is about 0.5 μm and that of NLP is about 0.25 μm (Figures 5D, F).

5 Discussion

5.1 Diagenetic controls on the formation of AHP

The complex and variable interplay of factors, such as the detrital composition, grain texture and prolonged diagenetic alteration after sediment deposition, yields a wide range of potential outcomes with respect to the pore structure and reservoir quality (Ajdukiewicz and Lander, 2010; Taylor, et al., 2010; Lai et al., 2018; Griffiths et al., 2019; Quandt et al., 2022; Wu et al., 2022; Marghani et al., 2023). There is no significant difference in the grain size and composition among the AHP, NHP, and NLP reservoirs in the AHPZ (Figures 6A, B). The average sorting coefficient of the AHP is the lowest among these sandstone reservoirs, with an average of 1.9 (Figure 6A). Correspondingly, the average initial porosity (32.9%) is the largest. However, the difference between the average initial porosity of AHP sandstones and that of NHP and NLP sandstones is 1.5% and 2.8% (Beard and Weyl, 1973), respectively. Therefore, the sedimentation differentiation may have no significant controls on the formation of AHP sandstone reservoirs in the AHPZ.

5.1.1 Compaction

Compaction is a collection of processes that lead to both the intergranular volume (IGV) and primary porosity decrease with increasing burial depth. The grain contacts of J_2x^{1+2} sandstones mainly vary from point to linear contact (Figures 4A–C), indicating that the degree of compaction is significantly different among the AHP, NHP, and NLP sandstones in the AHPZ. The IGV of sediment can be measured to evaluate the degree of sandstone compaction (Houseknecht, 1987; Paxton et al., 2002). Assuming that the initial porosity of the well-sorted J_2x^{1+2} sandstone is about 40%, the porosity loss rate caused by compaction is distributed from 64.8% to 99.5% with an average of 89.6%, which reveals that the compaction plays a most important role in porosity loss for J_2x^{1+2} sandstone (Figure 7A). The strong degree of compaction of the J_2x^{1+2} sandstone is due to the progressive burial in which the early burial rate is greater than the late burial rate (Wu and Zhao, 1997; Shao et al., 2003). In addition, the abundance of acidic fluids in the coal measure strata during the early diagenesis makes the dissolution of clastic particles common, which in turn reduces the compaction resistance of the sandstone (Shou et al., 2006).

The NHP and NLP sandstones underwent more extensive compaction, resulting in a >90% reduction in initial porosity. However, the AHP sandstones in the same AHPZ underwent a less 80% reduction in initial porosity through compaction (Figure 7A). The factors responsible for the difference in the rates and degrees of sandstone compaction mainly focus on the following two aspects: 1) Internal factors involving sediment composition and texture (Taylor et al., 2010; Tobin et al., 2010); and 2) External factors induced by temperature, stress condition, and burial rate (Pittman and Larese, 1991; Shou et al., 2006). The composition and grain size cannot explain the differential compaction of AHP, NHP and NLP sandstone reservoirs (Figures 6A, B). However, the mechanical compaction of poorly sorted NLP sandstones that have the maximum sorting coefficient will be extensive (Figures 6A, 7B). This is because the pores between the relatively large particles are easy to be filled by smaller particles (Mckinley et al., 2011). When the sorting coefficient is <2, the NHP and AHP sandstone reservoirs co-exist (Figure 7B), signifying that the sorting coefficient is not the sole factor controlling the compaction rate. The tectonic stress condition may be responsible for most intergranular porosity preservation in the AHP sandstones. The nappe tectonics developed in the Qiketai—Huoyanshan area of the Turpan-Hami Basin can alleviate

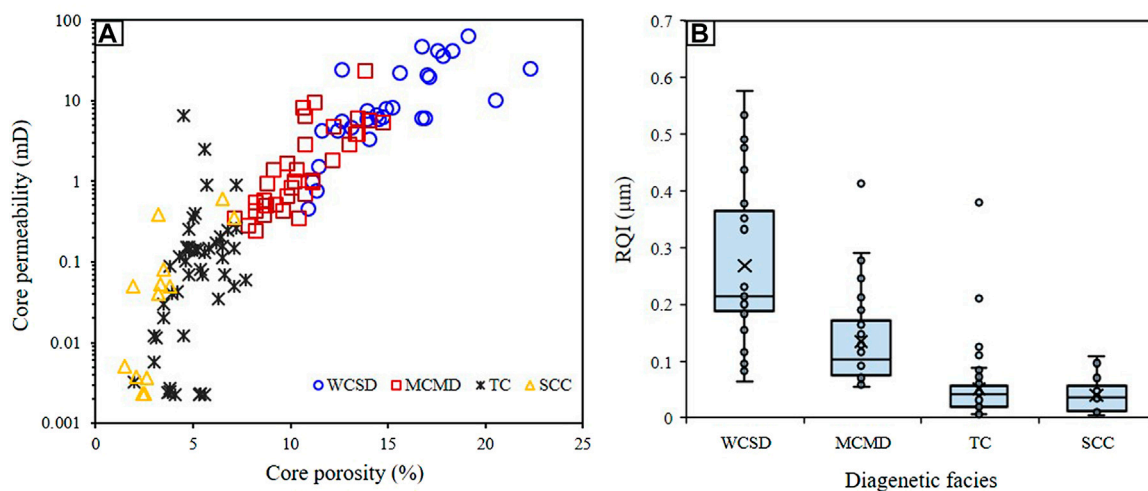


FIGURE 10

(A) The porosity-permeability cross plots of the various diagenetic facies. (B) Box-whisker plots viewing the variance in RQI among various diagenetic facies. The legend is the same as Figure 6.

the compaction to a certain extent (Figure 8), thus reducing the compaction rate and preserving the IGV of sandstones under the nappe (Shou et al., 2005). Taking well K31 in the northern piedmountain zone, well J3 in the abdominal zone and well H803 in the southern nappe tectonic zone as examples, the compaction of well H803 sandstone is significantly weaker than that in other zones when the depth is similar, as confirmed by thin section images (Figures 4A–C). The sandstone porosity and permeability of well H803 at a depth of 4002.45 m can reach 12.6% and 5.688 mD, respectively. The primary porosity with good connectivity is up to 65%, which accounts for the relatively high permeability of the sandstone reservoir.

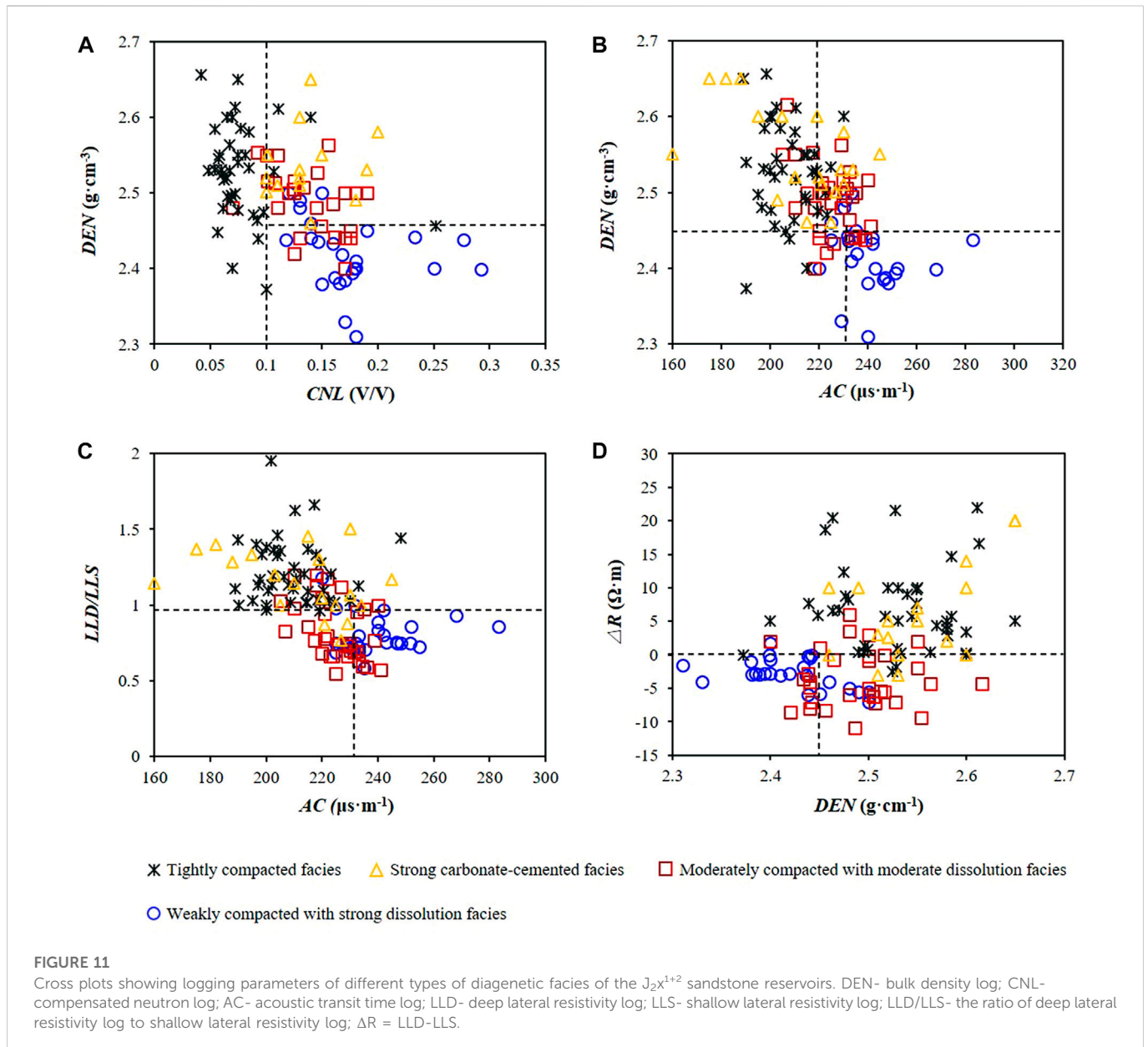
5.1.2 Cementation

Different types of cements can be observed in the J_2x^{1+2} sandstone (Figure 4). The cements are mainly carbonate, followed by clay minerals, with less quartz cement. The porosity loss destroyed by cementation ranges from 0.1% to 11.6% (avg 1.42%), accounting for 0.2%–28.9% (avg 3.55%) of IGV in the J_2x^{1+2} sandstones (Figure 7A). The porosity lost by cementation in the AHP sandstone varies from 0.3% to 3.5%, with an average of 0.94%. The corresponding values for the NHP and NLP sandstone reservoirs are 0.3%–8.4%, 1.39%, and 0.1%–11.6%, and 1.64%, respectively (Figure 7A). There is no significant difference in the content of carbonate cements among AHP, NHP, and NLP sandstones (Figure 6C), indicating that the carbonate cement are not the main factor affecting the formation of AHP sandstone. It is worth noting that there are more outliers in the distribution of carbonate cements in NLP sandstones than in AHP and NHP sandstones (Figure 6C). The poikilitic calcites filling large intergranular spaces are responsible for these outliers, which is confirmed by thin section observations (Figure 4G). Therefore, in addition to the tight compaction (Figure 7A), the strong carbonate cementation is also the main reason for the formation of the NLP sandstones. Although the content of authigenic clay minerals is low, the content of different types of clay minerals is significantly different in AHP, NHP, and NLP sandstones (Figure 6C). The contents of

kaolinite and chlorite are relatively higher in the AHP and NHP sandstones, while the contents of illite and I/S mixed layer are relatively higher in the NLP sandstones. The illite and I/S mixed layer generally occurred as pore-filling forms, which clogs the pore systems and thus attenuates the reservoir quality. The chlorite occurred as grain coatings, which plays a positive role in preserving intergranular pores and improving reservoir quality (Zhou et al., 2016). Compared with the NLP sandstone, more intergranular pores preserved in the AHP and NHP sandstones can provide conduits for acidic fluid transport to enhance dissolution, which leads to a marked increase in content of authigenic kaolinite (Surdam et al., 1989).

5.1.3 Dissolution

The dissolution of framework grains significantly increases the porosity and thus promotes the formation of the AHPZ (Figure 3). The secondary dissolution pores mainly occur in the AHP sandstones, followed by the NHP and NLP sandstones. The point-counting results show that the secondary thin-section porosity of AHP sandstone ranges from 3.0% to 7.0%, with an average of 4.9%. The corresponding values for NHP and NLP sandstones are 2.0%–6.0%, 3.8% and 0.2%–4.0%, 2.5%, respectively. The J_2x^{1+2} sandstones are located adjacent to coals and dark mudstones, which are in the stages of low maturity to maturity (Table 1). The organic acids released by coal-bearing source rocks provide conditions for the dissolution of J_2x^{1+2} sandstones. The results also indicate that the dissolution is closely related to the development degree of intergranular pores after compaction and cementation (Li et al., 2020; Wu et al., 2022). There is a significant positive correlation between the primary and secondary thin-section porosity (Figure 9A). This is because the intergranular pores served as the main pathway for fluid activity (Li et al., 2020). The contribution of secondary porosity in the AHP sandstone to core porosity and permeability is more significant than that in NHP and NLP sandstones (Figures 9B, C). The PSD of the AHP sandstone is significantly higher than that of the NHP and NLP sandstones (Figure 5), which may allow by-products of



dissolution to be effectively carried away from the dissolution minerals, thus effectively increasing the porosity and permeability.

5.2 Implications for reservoir quality prediction

5.2.1 Association of AHP, NHP, and NLP with diagenetic facies and their log responses

The differential reservoir quality of AHP, NHP, and NLP sandstones within the AHPZ can be explained by the various diagenetic facies. Based on the complex diagenetic processes, diagenetic minerals, and pore systems (Lai et al., 2018), the four main types of diagenetic facies, i.e., strong carbonate-cemented facies (SCC), tightly compacted facies (TC), moderately compacted with moderate dissolution facies (MCMD), and weakly compacted with strong dissolution facies (WCSD), are

distinguished in the J_2x^{1+2} sandstones. The SCC and TC are the destructive diagenetic facies that tend to form NLP sandstones with a poor reservoir quality in the Taibei sag (Figures 4G, 8C). The MCMD has a moderate reservoir quality and eventually forms the NHP sandstones (Figures 4B, C). The WCSD is an important construction diagenetic facies for the best reservoir quality layers, which mainly corresponds to the AHP sandstones (Figures 4A, 8A). The AHP and NHP sandstones are defined as relatively high-quality sandstone reservoirs (Wu et al., 2022). Additionally, significant differences exist in the porosity and permeability of sandstone reservoirs with different types of diagenetic facies (Figure 10A). The reservoir quality index (RQI) is a valid proxy for evaluating the reservoir quality heterogeneity, and the corresponding equation is written as $RQI(\mu m) = 0.0314\sqrt{K/\Phi}$ (where K is the permeability, μm^2 ; Φ is the porosity, fraction) (Amaefule et al., 1993). The RQI of the WCSD is the highest, followed by the MCMD, while the TC and SCC are the worst (Figure 10B).

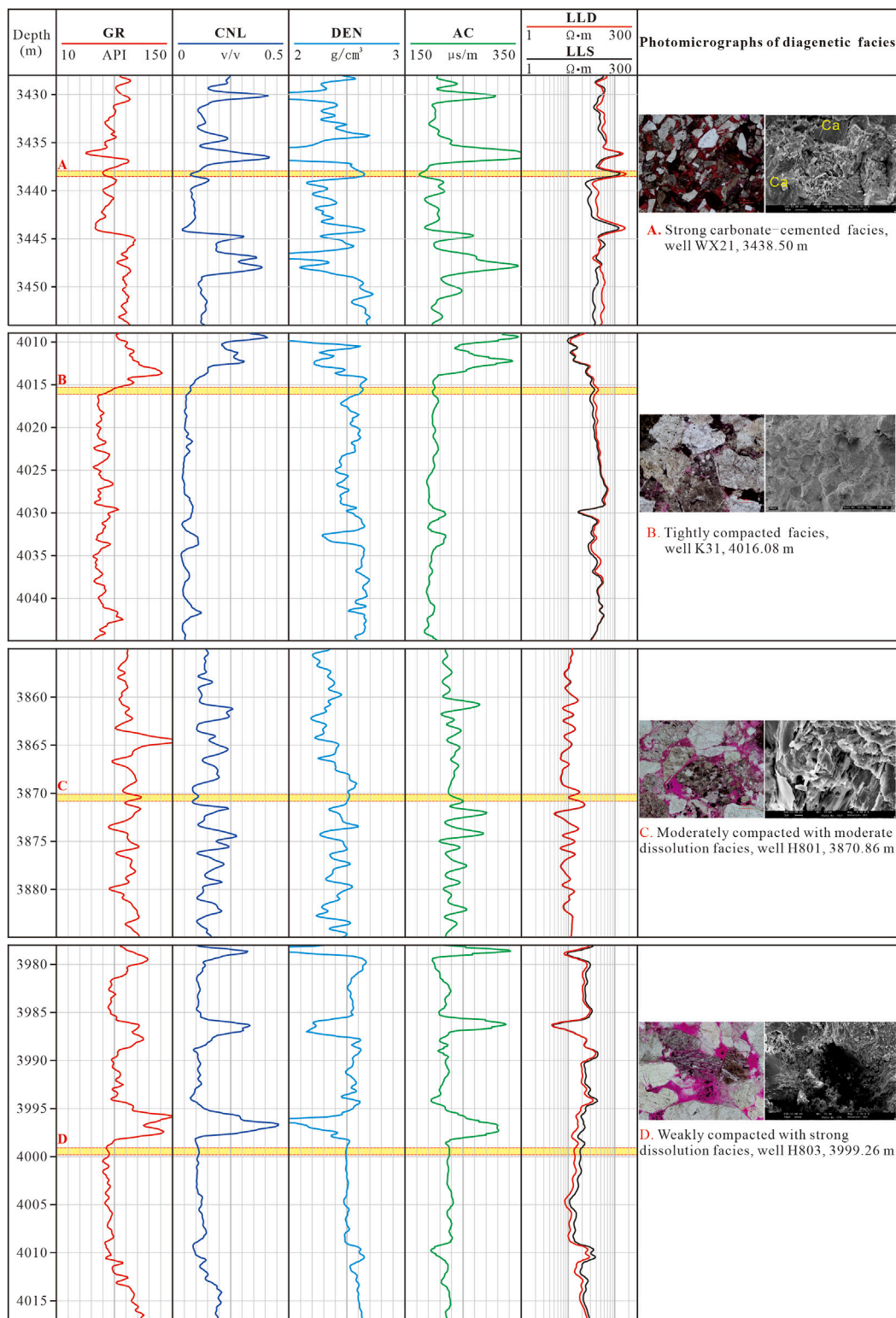


FIGURE 12
The typical photomicrographs and corresponding well log responses of different types of diagenetic facies.

Therefore, correlating the AHP, NHP, and NLP sandstones to the different types of diagenetic facies can be rationally used to predict the subsurface reservoir quality and thus evaluate the favorable reservoir intervals (Ozkan et al., 2011; Lai et al., 2018).

The conventional well logs, such as compensated neutron log (CNL), bulk density log (DEN), acoustic transit time log (AC), deep lateral resistivity log (LLD) and shallow lateral resistivity log (LLS), are sensitive to changes in the diagenetic facies (Cui et al.,

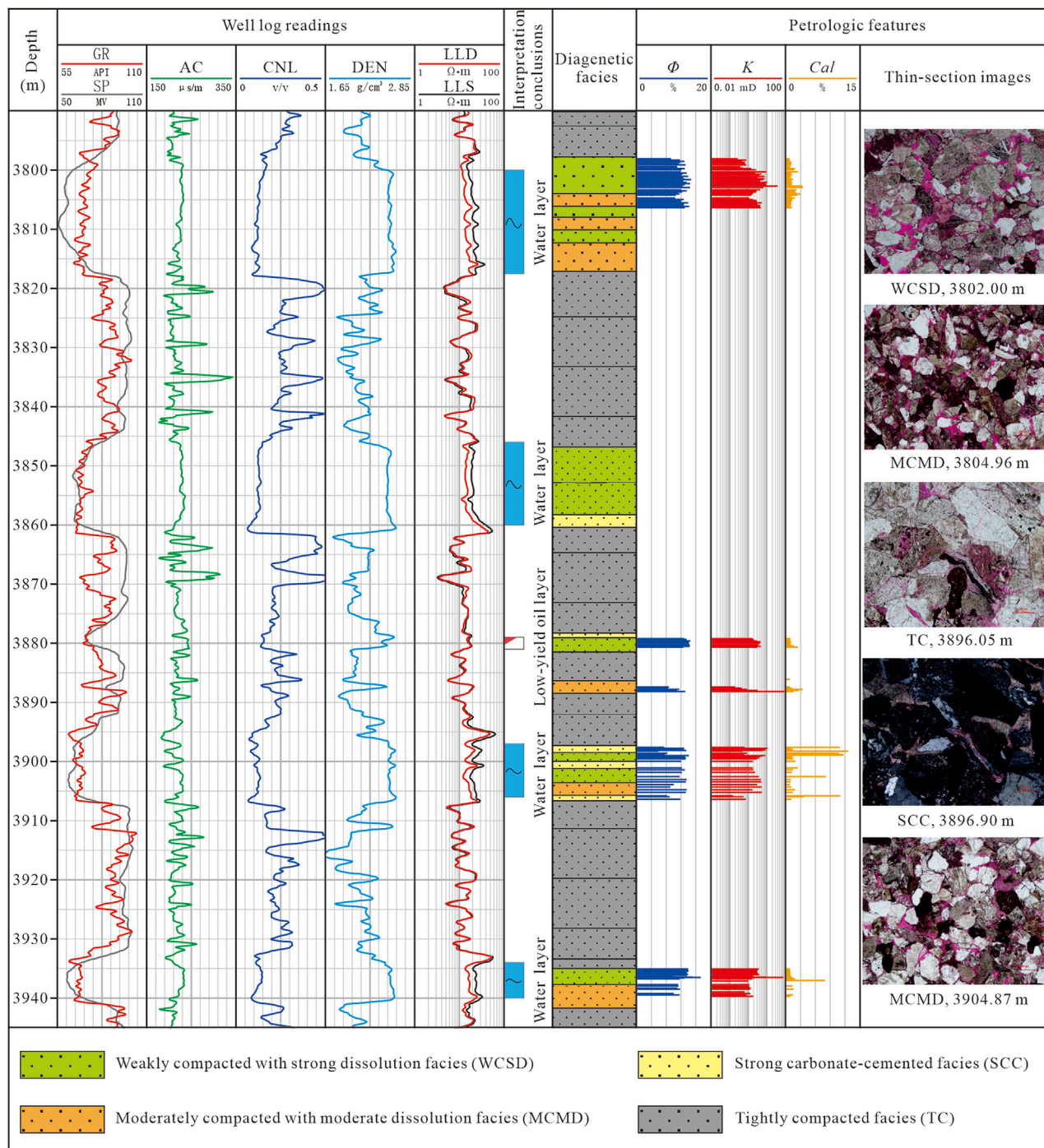


FIGURE 13
 Prediction of diagenetic facies in the vertical profile of well PB103. Φ -core porosity; K -core permeability; Cal -carbonate cement.

2017; Lai et al., 2018). The value of LLD minus LLS is defined as ΔR . The cross plots between the diagenetic facies of core sandstone samples and the corresponding calibrated well log values show that the different types of diagenetic facies have good differentiation in the well log responses (Figure 11). The well log responses of TC can be recognized by $\Delta R > 0$, high DEN values but low CNL and AC values (Figure 12A). The SCC has high DEN values, medium to high CNL values, low AC values and $\Delta R > 0$ (Figure 12B). The MCMD is characterized by the relatively

medium to high DEN, AC and CNL values, but $\Delta R < 0$ (Figure 12C). The WCSD has relatively high AC and CNL values, low DEN values and $\Delta R < 0$ (Figure 12D).

5.2.2 Prediction of reservoir quality via well log readings

The logging interpretation could provide the ultimate state of the various diagenetic facies that associated with the reservoir quality heterogeneity. A combination of well log readings discussed in

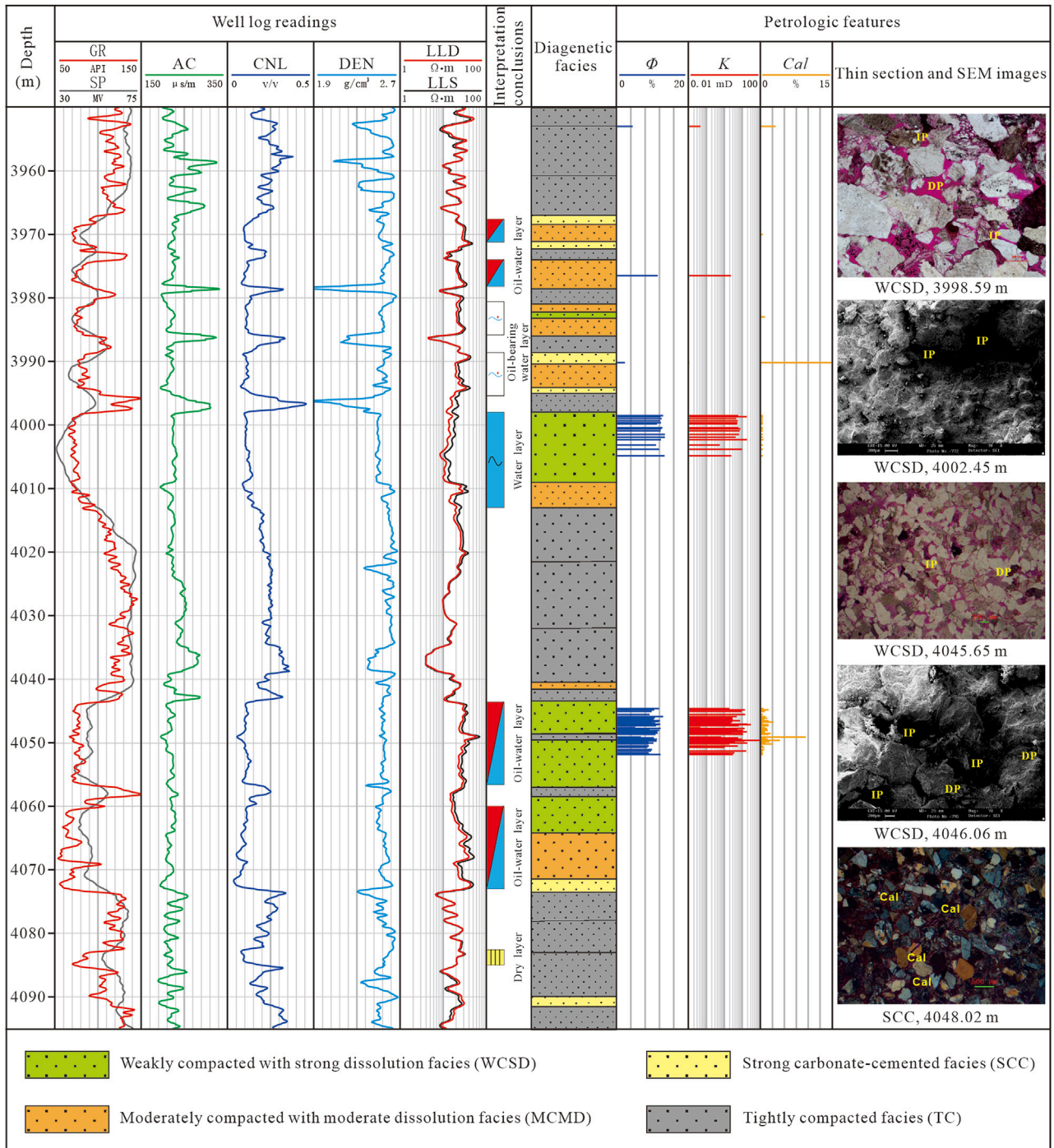


FIGURE 14 Prediction of diagenetic facies in the vertical profile of well H803. Φ-core porosity; K-core permeability; Cal-carbonate cement.

subsection 5.2.1 can be used for identifying the diagenetic facies and thus predicting the reservoir quality of intervals that lack core control. A blind test has been performed on the intervals from other wells that were not involved in the model construction to verify the rationality of the constructed logging response model. Taking the wells PB102 and H803 as examples, the prediction of diagenetic facies in these wells are consistent with the results of thin section and SEM observations and physical property tests (Figures 13, 14), indicating that the constructed

well logging response chart can be used as an effective method to identify the diagenetic facies and thus predict the reservoir quality. In general, the oil-water, water and oil-bearing water layers are closely related to WCSD and MCMD, while the dry layers are associated with the TC (Figures 13, 14). The SCC with poor RQI occurs near the sand-mudstone contact surface. In addition, the constructed well log response charts are of great significance for the prediction of deeply buried favorable sandstones. The

interpretation of diagenetic facies reveals that relatively high-quality reservoirs are still developed in the lower Jurassic sandstones with depths larger than 4000 m (Figure 14), which has been confirmed by previous studies (Hao et al., 2020; Chen et al., 2022; He et al., 2022). It is worth noting that the logging response characteristics of the constructed diagenetic facies are different from the results of previous studies (Cui et al., 2017; Wu et al., 2020; Li et al., 2022), which may be due to the difference in tectonic setting, sedimentary environment, and diagenetic history. Correlating the diagenetic facies with well logs can provide a feasible perspective for quality evaluation, prediction, and classification of subsurface sandstone reservoirs, especially for deeply buried tight sandstone reservoirs.

6 Conclusion

- (1) The J_2x^{1+2} sandstones are mostly feldspathic litharenites and litharenites, which are characterized by moderate-to good sorting, silty to medium granularity, and point-to long grain contacts.
- (2) The J_2x^{1+2} sandstones have low porosity (avg 6.0%) and permeability (avg 1.12 mD), but show anomalously high measurements at depth interval of 3850–4050 m.
- (3) There is a noticeable variation in pore types and sizes from intergranular-intragranular dissolution pores with a size mode of 2.0 μm in AHP sandstones, to major intragranular dissolution pores with a size mode of 0.5 μm in NHP sandstones, to most micropores with a size mode of 0.25 μm occurred in the NLP sandstones.
- (4) Compaction is the main cause of reservoir quality attenuation, resulting in an average porosity loss of 89.6%. However, authigenic minerals have relatively little influence on reservoir quality, but poikilitic carbonate cements can generally form NLP sandstones.
- (5) The combination of nappe tectonics and well-sorted particles alleviated the compaction and thus preserved more intergranular pores in the AHP sandstones. Dissolution further increases the porosity and eventually forms the AHP sandstones.
- (6) The sandstones with strong carbonate-cemented facies (SCC) and tightly compacted facies (TC) are recognized as the NLP reservoirs. The moderately compacted with moderate dissolution facies (MCMD) and weakly compacted with strong dissolution facies (WCSD) correspond to NHP and AHP reservoirs, respectively.
- (7) The reservoir quality predicted using the constructed diagenetic facies charts is in good agreement with the photomicrograph observations and physical property tests. Additionally, the AHP reservoirs are still developed in the deeply buried sandstones with depths larger than 4000 m.

References

- Aase, N. E., Bjorkum, P. A., and Nadeau, P. H. (1996). The effect of grain-coating microquartz on preservation of reservoir porosity. *AAPG Bull.* 80, 1654–1673.
- Ajdukiewicz, J. M., and Lander, R. H. (2010). Sandstone reservoir quality prediction: The state of the art. *AAPG Bull.* 94, 1083–1091. doi:10.1306/intro060110

Data availability statement

The original contributions presented in the study are included in the article/supplementary material, further inquiries can be directed to the corresponding author.

Author contributions

HaW: Preparation, creation and presentation of the published work, specifically writing the initial draft. SB: Conducting the research and investigation process, specifically performing the experiments, or data/evidence collection. ZD: Analysis and/or interpretation of data. AH and JL: Revising the manuscript critically for important intellectual content. GW and HZ: Provide samples and partial data. YZ, HeW, and ML: Drawings and data collection.

Funding

This study was financially supported by the Fundamental Research Funds for the Central Universities (No. lzujbky-2021-17), the National Natural Science Foundation of China (No. 42202135), the Gansu Province Youth Science and Technology Fund Project (No. 20JR5RA226) and Fundamental Research Program of Shanxi Province (No. 202103021223283). The authors thank PetroChina Tuha Oilfield Company for their support in completing this study and permission to publish the results.

Conflict of interest

AH and JL were employed by the company PetroChina Research Institute of Petroleum Exploration & Development.

GW and HZ were employed by the company Exploration and Development Research Institute, PetroChina Tuha Oilfield Company.

The remaining authors declare that the research was conducted in the absence of any commercial or financial relationships that could be construed as a potential conflict of interest.

The authors declare that this study received funding from PetroChina. The funder had the following involvement in the study: collection and interpretation of data, and the decision to submit it for publication.

Publisher's note

All claims expressed in this article are solely those of the authors and do not necessarily represent those of their affiliated organizations, or those of the publisher, the editors and the reviewers. Any product that may be evaluated in this article, or claim that may be made by its manufacturer, is not guaranteed or endorsed by the publisher.

Allen, M. B., Sengör, A. M. C., and Natal'in, B. A. (1995). Junggar, Turfan and Alakol basins as late Permian to early Triassic extensional structures in a sinistral shear zone in the Altaid orogenic collage, Central-Asia. *J. Geol. Soc. Lond.* 152, 327–338. doi:10.1144/gsjgs.152.2.0327

Amaefule, J., Altunbay, M., Tiab, D., Kersey, D., and Keelan, D. (1993). "Enhanced reservoir description: Using core and log data to identify hydraulic (flow) units and predict

- permeability in uncored intervals/wells," in *68th annual tech. Conf. And exhibit* (Houston, TX, 1–16. Paper SPE26435.
- Amireh, B. S. (2015). Grain size analysis of the Lower Cambrian–Lower Cretaceous clastic sequence of Jordan: Sedimentological and paleo-hydrodynamical implications. *J. Asian Earth Sci.* 97, 67–88. doi:10.1016/j.jseas.2014.09.029
- Beard, D., and Weyl, P. (1973). Influence of texture on porosity and permeability of unconsolidated sand. *AAPG Bull.* 57, 349–369.
- Bjørlykke, K., and Jahren, J. (2012). Open or closed geochemical systems during diagenesis in sedimentary basins: Constraints on mass transfer during diagenesis and the prediction of porosity in sandstone and carbonate reservoirs. *AAPG Bull.* 96, 2193–2214. doi:10.1306/04301211139
- Bloch, S., Lander, R., and Bonnell, L. (2002). Anomalously high porosity and permeability in deeply buried sandstone reservoirs: Origin and predictability. *AAPG Bull.* 86, 301–328.
- Cao, Y. C., Yuan, G. H., Li, X. Y., Wang, Y. X., Xi, K. L., Wang, X. M., et al. (2014). Characteristics and origin of abnormally high porosity zones in buried Paleogene clastic reservoirs in the Shengtuo area, Dongying Sag, East China. *Petrol. Sci.* 11, 346–362. doi:10.1007/s12182-014-0349-y
- Carroll, A. R., Liang, Y. H., Graham, S. A., Xiao, X. C., Hendrix, M. S., Chu, J. C., et al. (1990). Junggar basin, northwest China: Trapped late paleozoic ocean. *Tectonophysics* 181, 1–14. doi:10.1016/0040-1951(90)90004-r
- Chen, J. P., Qin, Y., Huff, B. G., Wang, D. R., Han, D. X., and Huang, D. F. (2001). Geochemical evidence for mudstone as the possible major oil source rock in the Jurassic Turpan Basin, Northwest China. *Org. Geochem.* 32 (9), 1103–1125. doi:10.1016/s0146-6380(01)00076-6
- Chen, X., Wang, J. F., Xiao, D. S., Liu, J. T., Gou, H. G., Zhang, H., et al. (2022). Accumulation conditions and exploration direction of lower Jurassic tight sandstone gas reservoir in Taibei Sag. *Xinjiang Petrol. Geol.* 43 (5), 505–512. (in Chinese with English abstract).
- Clarkson, C. R., Solano, N., Bustin, R. M., Bustin, A. M. M., Chalmers, G. R. L., He, L., et al. (2013). Pore structure characterization of North American shale gas reservoirs using USANS/SANS, gas adsorption, and mercury intrusion. *Fuel* 103, 606–616. doi:10.1016/j.fuel.2012.06.119
- Cui, Y. F., Wang, G. W., Jones, S. J., Zhou, Z. L., Ran, Y., Lai, J., et al. (2017). Prediction of diagenetic facies using well logs—a case study from the upper Triassic Yanchang Formation, Ordos Basin, China. *Mar. Pet. Geol.* 81, 50–65. doi:10.1016/j.marpetgeo.2017.01.001
- Desbois, G., Urai, J. L., Kukla, P. A., Konstanty, J., and Baerle, C. (2011). High-resolution 3D fabric and porosity model in a tight gas sandstone reservoir: A new approach to investigate microstructures from mm- to nm-scale combining argon beam cross-sectioning and SEM imaging. *J. Pet. Sci. Eng.* 78, 243–257. doi:10.1016/j.petrol.2011.06.004
- Dickson, J. A. D. (1965). A modified staining technique for carbonates in thin section. *Nature* 205, 587. doi:10.1038/205587a0
- Ehrenberg, S. N. (1989). Assessing the relative importance of compaction processes and cementation to reduction of porosity in sandstones: Discussion; compaction and porosity evolution of pliocene sandstones, ventura basin, California: Discussion. *AAPG Bull.* 73, 1274–1276.
- Emery, D., Smalley, P. C., Oxtoby, N. H., Ragnarsdottir, K. V., Aagaard, P., Halliday, A., et al. (1993). Synchronous oil migration and cementation in sandstone reservoirs demonstrated by quantitative description of diagenesis. *Phil Trans. R. Soc. Lond. A* 344, 115–125.
- Folk, R. L. (1980). *Petrology of sedimentary rocks*. Austin, Texas: Hemphill Publishing, 182.
- Gao, G., Yang, S. R., Liang, H., Wang, Z. Y., and Li, X. N. (2018). The origin and secondary alteration of dissolved gas in oil: A case study from the Western tu-ha basin, China. *J. Nat. Gas. Sci. Eng.* 52, 283–294. doi:10.1016/j.jngse.2018.01.044
- Gluyas, J., and Coleman, M. (1992). Material flux and porosity changes during sediment diagenesis. *Nature* 356, 52–54. doi:10.1038/356052a0
- Greene, T. J., Carroll, A. R., Wartes, M., Graham, S. A., and Wooden, J. L. (2005). Integrated provenance analysis of a complex orogenic terrane: Mesozoic uplift of the Bogda Shan and inception of the Turpan-Hami Basin, NW China. *J. Sediment. Res.* 75, 251–267. doi:10.2110/jsr.2005.019
- Greene, T. J., Zinniker, D., Moldowan, J. M., Cheng, K. M., and Su, A. G. (2004). Controls of oil family distribution and composition in nonmarine petroleum systems: A case study from the Turpan-Hami Basin, northwestern China. *AAPG Bull.* 88, 447–481. doi:10.1306/10270303015
- Griffiths, J., Worden, R. H., Wooldridge, L. J., Utley, J. E. P., Duller, R. A., and Edge, R. L. (2019). Estuarine clay mineral distribution: Modern analogue for ancient sandstone reservoir quality prediction. *Sedimentology* 66, 2011–2047. doi:10.1111/sed.12571
- Han, S. B., Zhang, J. C., Zhou, Y. Q., Bai, S. T., Huang, L. X., Wang, C. S., et al. (2016). Formation and accumulation of lower Jurassic tight gas sands field in Kekeya area of Tuha Basin, northwestern China. *J. Nat. Gas. Sci. Eng.* 29, 101–109. doi:10.1016/j.jngse.2015.12.046
- Hao, A. S., Li, J., Guo, J. Y., Ran, Q. G., Zhang, H., Qi, X. N., et al. (2020). Provenance and depositional systems of the second member of lower jurassic Sangonghe Formation in Taibei sag, Turpan-Hami Basin, China. *J. China U. Min. Technol.* 50, 893–908. (in Chinese with English abstract).
- Hao, A. S., Li, J., Guo, J. Y., Wu, H., Ran, Q. G., Li, Z. S., et al. (2022). Characteristics and exploration direction of tight sandstone gas reservoirs in the Lower Jurassic of Turpan-Hami Basin. *Nat. Gas. Geosci.* 32, 1212–1222. (in Chinese with English abstract).
- Hao, A. S., Wu, H., Ran, Q. G., Li, J., Guo, J. Y., Ban, S. Y., et al. (2021). Development characteristics and Genesis of secondary high porosity zones in deep clastic reservoir: A case study of the lower jurassic in the Taibei sag of the Tuha basin. *Nat. Gas. Ind.* 40, 50–59. (in Chinese with English abstract).
- He, H. Q., Liang, S. J., Guo, X. J., Luo, Q. S., Wang, J. F., Chen, X., et al. (2022). New discoveries and exploration prospects of Middle and Lower Jurassic lithologic reservoirs in depression area of Turpan-Hami Basin. *Nat. Gas. Geosci.* 33 (7), 1025–1035. (in Chinese with English abstract).
- Heald, M. T., and Larese, R. E. (1974). Influence of coatings on quartz cementation. *J. Sediment. Petrol.* 44, 1269–1274.
- Hillier, S. (2003). "Quantitative analysis of clay and other minerals in sandstones by X-ray powder diffraction (XRPD)," in *Clay mineral cements in sandstones*. Editors R. Worden and S. Morad (Oxford, International: International Association of Sedimentologist, Special Publication), 213–251.
- Houseknecht, D. W. (1987). Assessing the relative importance of compaction processes and cementation to reduction of porosity in sandstones. *AAPG Bull.* 71, 633–642.
- Ji, H. J., Tao, H. F., Wang, Q., Qiu, Z., Ma, D. X., Qiu, J. L., et al. (2017). Early to Middle Jurassic tectonic evolution of the Bogda mountains, Northwest China: Evidence from sedimentology and detrital zircon geochronology. *J. Asian Earth Sci.* 153, 57–74. doi:10.1016/j.jseas.2017.03.018
- Jin, Z. K., Su, K., and Su, N. N. (2011). Origin of Jurassic deep burial high-quality reservoirs in the central Junggar Basin. *Acta Petrol. Sin.* 32, 25–31. (In Chinese with English abstract).
- Lai, J., Wang, G., Wang, S., Cao, J., Li, M., Pang, X., et al. (2018). Review of diagenetic facies in tight sandstones: Diagenesis, diagenetic minerals, and prediction via well logs. *Earth-Science Rev.* 185, 234–258. doi:10.1016/j.earscirev.2018.06.009
- Law, J., and Curtis, J. B. (2002). Introduction to unconventional petroleum systems. *AAPG Bull.* 86, 1851–1852.
- Li, M., Guo, Y. H., Li, Z. F., and Wang, H. C. (2020). The diagenetic controls of the reservoir heterogeneity in the tight sand gas reservoirs of the zizhou area in China's east ordos basin: Implications for reservoir quality predictions. *Mar. Petrol. Geol.* 112, 104088. doi:10.1016/j.marpetgeo.2019.104088
- Li, T. J., Huang, Z. L., Zhao, J., Xu, X. F., and Guo, X. B. (2021). Pore structure characteristics and their influencing factors: A case study from the middle jurassic mixed siliciclastic carbonate rocks, Turpan-Hami Basin, northwest China. *J. Petrol. Sci. Eng.* 203, 108611. doi:10.1016/j.petrol.2021.108611
- Li, Z. H., Zhang, L. Q., Yuan, W. F., Chen, X., Zhang, L., and Li, M. Q. (2022). Logging identification for diagenetic facies of tight sandstone reservoirs: A case study in the lower jurassic ahe formation, kuqa depression of tarim basin. *Mar. Petrol. Geol.* 139, 105601. doi:10.1016/j.marpetgeo.2022.105601
- Liang, S. J., Qian, F., and Xiao, D. S. (2022). Exploration discovery and implications of the jurassic tight sandstone oil and gas reservoir in well Ji7H in Taibei sag, Turpan-Hami Basin. *China Petrol. Dev.* 27, 50–59. (In Chinese with English abstract).
- Luo, L., Meng, W. B., Gluyas, J., Tan, X. F., Gao, X. Z., Feng, M. S., et al. (2019). Diagenetic characteristics, evolution, controlling factors of diagenetic system and their impacts on reservoir quality in tight deltaic sandstones: Typical example from the xujiahe Formation in western sichuan foreland basin, SW China. *Mar. Pet. Geol.* 103, 231–254. doi:10.1016/j.marpetgeo.2019.02.012
- Marghani, M. M. A., Zairi, M., and Radwan, A. E. (2023). Facies analysis, diagenesis, and petrophysical controls on the reservoir quality of the low porosity sandstone of the Nubian formation, east Sirt Basin, Libya: Insights into the role of fractures in fluid migration, fluid flow, and enhancing the permeability of low porous reservoirs. *Mar. Pet. Geol.* 147, 105986. doi:10.1016/j.marpetgeo.2022.105986
- Mckinley, J. M., Atkinson, P. M., Lloyd, C. D., Ruffell, A. H., and Worden, R. H. (2011). How porosity and permeability vary spatially with grain size, sorting, cement volume, and mineral dissolution in fluvial triassic sandstones: The value of geostatistics and local regression. *J. Sediment. Res.* 81, 844–858. doi:10.2110/jsr.2011.71
- Nguyen, B. T. T., Jones, S. J., Gouly, N. R., Middleton, A. J., Grant, N., Ferguson, A., et al. (2013). The role of fluid pressure and diagenetic cements for porosity preservation in Triassic fluvial reservoirs of the Central Graben, North Sea. *AAPG Bull.* 97, 1273–1302. doi:10.1306/01151311163
- Ni, Y. Y., Liao, F. R., Gong, D. Y., Jiao, L. X., Gao, J. L., and Yao, L. M. (2019). Stable carbon and hydrogen isotopic characteristics of natural gas from Taibei Sag, Turpan-Hami Basin, NW China. *Petrol. explore. Dev.* 46 (3), 531–542. doi:10.1016/s1876-3804(19)60033-9
- Nielsen, M. T., Weibel, R., Therkelsen, J., and Friis, H. (2019). Distribution of porosity-preserving microquartz coatings in sandstones, upper jurassic Danish central graben. *Geol. Surv. Den. Greenl. Bull.* 43, e2019430103. doi:10.34194/geusb-201943-01-03
- Ozkan, A., Cumella, S. P., Milliken, K. L., and Laubach, S. E. (2011). Prediction of lithofacies and reservoir quality using well logs, late cretaceous williams fork formation, mamm creek field, piceance basin, Colorado. *AAPG Bull.* 95, 1699–1723. doi:10.1306/01191109143
- Paxton, S. T., Szabo, J. O., Ajdukiewicz, J. M., and Klimentides, R. E. (2002). Construction of an intergranular compaction curve for evaluating and predicting compaction and porosity loss in rigid grained sandstone reservoirs. *AAPG Bull.* 86, 2047–2067.

- Pittman, E. D., and Larese, R. E. (1991). Compaction of lithic sands: Experimental results and applications. *AAPG Bull.* 75, 1279–1299.
- Quandt, D., Busch, B., Schmidt, C., and Hilgers, C. (2022). Diagenesis and controls on reservoir quality of Lower Triassic red bed sandstones (Buntsandstein) from a marginal basin facies, southwest Germany. *Mar. Pet. Geol.* 142, 105744. doi:10.1016/j.marpetgeo.2022.105744
- Schmidt, V., and McDonald, D. A. (1979). The role of secondary porosity in the course of sandstone diagenesis. *SEPM Spec. Publ.* 26, 175–207. doi:10.2110/pec.79.26.0175
- Shao, L. Y., Zhang, P. F., Hilton, J., Gayer, R., Wang, Y. B., Zhao, C. Y., et al. (2003). Paleoenvironments and paleogeography of the late mesozoic and lower Middle Jurassic coal measures in the Turpan-Hami oil-prone coal basin, northwestern China. *AAPG Bull.* 87, 335–355. doi:10.1306/09160200936
- Shen, T. Y., Chen, Y., Wang, G. C., Ji, J. L., Wang, Y., Zhang, P., et al. (2020). Detrital zircon geochronology analysis of the late mesozoic deposition in the Turpan-Hami Basin: Implications for the uplift history of the eastern tian Shan, north-Western China. *Terra nova.* 32, 166–178. doi:10.1111/ter.12445
- Shou, J. F., Zhang, H. L., Shen, Y., Wang, X., Zhu, G. H., and Si, C. S. (2006). Diagenetic mechanisms of sandstone reservoirs in China oil and gas-bearing basins. *Acta Petrol. Sin.* 22 (8), 2165–2170.
- Shou, J. F., Zhang, H. L., Si, C. S., Wang, X., Chen, Z., and Wang, S. (2005). *Dynamic diagenesis of sandstone*. Beijing: Petroleum Industry Press, 88–99. (in Chinese).
- Stroker, T. M., Harris, N. B., Elliott, C. W., and Wampler, J. M. (2013). Diagenesis of a tight gas sand reservoir: Upper cretaceous mesaverde group, piceance basin, Colorado. *Mar. Petrol. Geol.* 40, 48–68. doi:10.1016/j.marpetgeo.2012.08.003
- Sun, L. D., Zou, C. N., Zhu, R. K., Zhang, Y. H., Zhang, S. C., Zhang, B. M., et al. (2013). Formation, distribution and potential of deep hydrocarbon resources in China. *Petrol. explor. Dev.* 40, 687–695. doi:10.1016/s1876-3804(13)60093-2
- Surdam, R. C., Crossey, L. J., Hagen, E. S., and Heasler, H. P. (1989). Organic-inorganic interactions and sandstones diagenesis. *AAPG Bull.* 73, 1–23.
- Taylor, T. R., Giles, M. R., Hathon, L. A., Diggs, T. N., Braunsdorf, N. R., Birbiglia, G. V., et al. (2010). Sandstone diagenesis and reservoir quality prediction: Models, myths, and reality. *AAPG Bull.* 94, 1093–1132. doi:10.1306/04211009123
- Tian, J. Q., Liu, J. Z., Zhang, Z. B., and Cong, F. Y. (2017). Hydrocarbon-generating potential, depositional environments, and organisms of the middle permian tarlong Formation in the Turpan-Hami Basin, northwestern China. *Geol. Soc. Am. Bull.* 54, 1064–1080.
- Tobin, R. C., McClain, T., Lieber, R. B., Ozkan, A., Banfield, L. A., Marchand, A. M. E., et al. (2010). Reservoir quality modeling of tight-gas sands in Wamsutter field: Integration of diagenesis, petroleum systems, and production data. *AAPG Bull.* 94, 1229–1266. doi:10.1306/04211009140
- Wang, Y. Z., Cao, Y. C., Song, G. Q., and Sui, F. G. (2009). Determination of physical property lower limit of deep clastic effective reservoirs of Paleogene in Dongying Depression. *J. China Univ. Petrol.* 33, 16–21. (In Chinese with English abstract).
- Washburn, E. W. (1921). The dynamics of capillary flow. *Phys. Rev.* 17, 273–283. doi:10.1103/physrev.17.273
- Weibel, R., Olivarius, M., Jakobsen, F. C., Whitehouse, M., Larsen, M., Midtgaard, H., et al. (2019). Thermogenetic degradation of early zeolite cement: An important process for generating anomalously high porosity and permeability in deeply buried sandstone reservoirs? *Mar. Petrol. Geol.* 103, 620–645. doi:10.1016/j.marpetgeo.2019.02.006
- Worden, R. H., French, M. W., and Mariani, E. (2012). Amorphous silica nanoflms result in growth of misoriented microcrystalline quartz cement maintaining porosity in deeply buried sandstones. *Geology* 40, 179–182. doi:10.1130/g32661.1
- Wu, D., Liu, S. B., Chen, H. D., Lin, L. B., Yu, Y., Xu, C., et al. (2020). Investigation and prediction of diagenetic facies using well logs in tight gas reservoirs: Evidences from the xu-2 member in the xinchang structural belt of the Western sichuan basin, Western China. *J. Petrol. Sci. Eng.* 192, 107326. doi:10.1016/j.petrol.2020.107326
- Wu, H., Ji, Y. L., Du, Z. W., Zhou, Y., Zou, J., Zhang, Y. Z., et al. (2022). Evolution and controls of high reservoir quality in Oligocene sandstones from moderate to deep burial, Nanpu Sag, Bohai Bay Basin, China. *Sediment Geol.* 441, 106275. doi:10.1016/j.sedgeo.2022.106275
- Wu, T., and Zhao, W. Z. (1997). *Formation and distribution of coal measure oil-gas fields in Turpan-Hami Basin*. Beijing: Petroleum Industry Press. (in Chinese).
- Xia, C. Y., Wilkinson, M., and Haszeldine, S. (2020). Petroleum emplacement inhibits quartz cementation and feldspar dissolution in a deeply buried sandstone. *Mar. Petrol. Geol.* 118, 104449. doi:10.1016/j.marpetgeo.2020.104449
- Xia, L. Q., Xu, X. Y., Li, X. M., Ma, Z. P., and Xia, Z. C. (2012). Reassessment of petrogenesis of Carboniferous-Early Permian rift-related volcanic rocks in the Chinese Tianshan and its neighboring areas. *Geosci. Front.* 3, 445–471. doi:10.1016/j.gsf.2011.12.011
- Yuan, G. H., Cao, Y. C., Gluyas, J., Li, X. Y., Xi, K. L., Wang, Y. Z., et al. (2015b). Feldspar dissolution, authigenic clays, and quartz cements in open and closed sandstone geochemical systems during diagenesis: Typical examples from two sags in bohai bay basin, east China. *AAPG Bull.* 99, 2121–2154. doi:10.1306/07101514004
- Yuan, G. H., Cao, Y. C., Jia, Z. Z., Wang, Y. Z., and Yang, T. (2015a). Research progress on anomalously high porosity zones in deeply buried clastic reservoirs in petroliferous basin. *Nat. Gas. Geosci.* 26, 28–42. (In Chinese with English abstract).
- Zhai, G. M., Hu, J. Y., Zhao, W. Z., and Zou, C. N. (2016). History, achievements and significance of scientific exploration wells: For the 30th anniversary of the “scientific exploration well” program. *Petrol. explor. Dev.* 43, 167–181. doi:10.1016/s1876-3804(16)30021-0
- Zhang, J., Liu, G., Cao, Z., Tao, S., Felix, M., Kong, Y., et al. (2019). Characteristics and formation mechanism of multi-source mixed sedimentary rocks in a saline lake, a case study of the Permian Lucaogou Formation in the Jimusaer Sag, northwest China. *Mar. Petrol. Geol.* 102, 704–724. doi:10.1016/j.marpetgeo.2019.01.016
- Zhang, S. H., Wang, J. Q., Liu, C. Y., Bai, J. K., Peng, H., Huang, H. X., et al. (2018). Detrital zircon U-Pb geochronology of the Permian strata in the Turpan-Hami Basin in North Xinjiang, NW China: Depositional age, provenance, and tectonic implications. *Geol. J.* 54, 1064–1080. doi:10.1002/gj.3374
- Zhong, D. K., Zhu, X. M., Zhang, Z. H., and Zhang, Q. (2003). Origin of secondary porosity of Paleogene sandstone in the dongying sag. *Petrol. explor. Dev.* 30, 51–53.
- Zhou, Y., Ji, Y. L., Xu, L. M., Che, S. Q., Niu, X. B., Wan, L., et al. (2016). Controls on reservoir heterogeneity of tight sand oil reservoirs in Upper Triassic Yanchang Formation in Longdong Area, southwest Ordos Basin, China: Implications for reservoir quality prediction and oil accumulation. *Mar. Petrol. Geol.* 78, 110–135. doi:10.1016/j.marpetgeo.2016.09.006
- Zou, C. N., Yang, Z., Tao, S. Z., Yuan, X. J., Zhu, R. K., Hou, L. H., et al. (2013). Continuous hydrocarbon accumulation over a large area as a distinguishing characteristic of unconventional petroleum: The ordos basin, north-central China. *Earth-Sci. Rev.* 126, 358–369. doi:10.1016/j.earscirev.2013.08.006
- Zou, C. N., Zhu, R. K., Liu, K. Y., Su, L., Bai, B., Zhang, X. X., et al. (2012). Tight gas sandstone reservoirs in China: Characteristics and recognition criteria. *J. Pet. Sci. Eng.* 88, 82–91. doi:10.1016/j.petrol.2012.02.001